ORNL/TM-2024/214094

Report on use of Inoculants in Missile Application Alloys

Jaimie Tiley
Soumya Nag

March 2024

ORNL IS MANAGED BY UT-BATTELLE LLC FOR THE US DEPARTMENT OF ENERGY

OAK RIDGE National Laboratory

ORNL/TM-2024/214094

Materials Science and Technology Division

REPORT ON USE OF INOCULANTS IN MISSILE APPLICATION ALLOYS

Jaimie Tiley
Soumya Nag

MARCH 2024

Prepared by
OAK RIDGE NATIONAL LABORATORY
Oak Ridge, TN 37831
managed by
UT-BATTELLE LLC
for the
US DEPARTMENT OF ENERGY
under contract DE-AC05-00OR22725

CONTENTS

LIST OF FIGURES

LIST OF TABLES

ACKNOWLEDGMENTS

This work was supported by the US Department of Energy, and the National Nuclear Security Administration Office of Nonproliferation and Arms Control. Supporting technical advice was provided by Mr. Mike Uzzle, Dr. David Mitchell, and Dr. Peeyush Nandwana at Oak Ridge National Laboratory.

ABSTRACT

This report documents the status of current inoculant research relevant to missile application alloys and MTCR control language. The information is intended to provide data on current inoculants for us determining the current state of development and identifying potential research directions. Although there has been significant scientific research into the development and synthesis of inoculants, their current availability is limited is traditional powder inoculants employed during casting processes. However, research continues the development of complex oxides, ribbon materials, high entropy alloys, and other inoculant product forms, including the use of inoculants in the melt pools produced during additive manufacturing. Research to date has focused primarily on aluminum and steel alloys with emphasis on refining grain structures and evolving equiaxed morphologies while increasing strength and castability. The primary inoculants in steel and cast irons include TiN, SiC, FeSi75, and Ce which have increased strength properties. Chief inoculants for Al alloys often include TiC, SiC, Al3Sc(x) and TiB2 to aid in precipitation and refinement. Ti and Ni alloys have fewer research activities involving inoculants, although TiN, TiB, ZrN and LaB6 (for Ti alloys) and WC, Co3FeNb2, and CrFeNb (for Ni alloys) have been used. Sic, Al2O3, Mg and Ti are key inoculants for Mg alloys. Multiple cast alloys from each of the material classes demonstrated increased strength and performance properties using inoculants, with several approaching requirements applicable to missile service environments. The continued evolution of advanced manufacturing capabilities is making it easier to produce high temperature near net shape structural materials using inoculant powders. These shapes may include the geometric shapes addressed within the MTCR (tubes and limited wall thicknesses). The use of inoculants may enable further development of high temperature alloys into near net shapes traditionally produced via casting processes due to limited ductility. This may decrease material and manufacturing costs. In addition, inoculation provides controlled kinetics and achievable chemical segregation that enables potential for far-from equilibrium thermodynamic microstructures and chemistries that could provide new metastable alloy states and subsequent properties to address co-design engineering constraints, including needs for increased strength and ductility. It is recommended that specific material combinations within these alloy classes be carefully watched as the materials evolve, with controls aimed at those having material properties above current MTCR levels. This specifically includes the use of refractory inoculants in alloys, and the application of inoculants in high strength and high temperature alloys via additive manufacturing processes, with care to link capabilities to product forms similar to the current requirements on tube geometries and material feed stocks. The continued development of nanoparticle inoculants will increase strength and ductility of high strength castings and additive manufactured metallic components. For example, adding inoculants into the casting of maraging steels and other precipitation strengthened alloys may drastically elevate mechanical properties above the control limit of current regulations.

1. INTRODUCTION

Missile Material Requirements are complicated and dependent on specific components and sections of the system (fuselage, nozzle, control surfaces etc.). Because of sensitivity issues, this report will only reference public accessible documents, which although dated, still convey relevant information. The traditional missile design is shown in Figure 1[1]. For comparison, the Typhoon missile developed in the late 1950s and early 1960s was capable of Mach 4.2 at 55,000-100,000 ft. The missile used both cobalt and nickel super alloys and light-weight honeycomb construction. The combustion components were protected with a ZrO2 flamed sprayed coating, alloying control surface temperatures above 1125F

and propulsion component temperatures above 2000F [2]. Current operating temperatures for contemporary systems have greatly exceeded those experienced by the Typhon missile, due in large part to the use of thermal protective systems and ramjet/rocket boosted technologies. Details on the specific impacts of flight missions on missile structures have been detailed elsewhere [1]. In general, missile design requirements for increased velocity, range, and maneuverability have increased drag and temperature constraints as well as introduced additional strains on structures. For example, Figure 2 provides top level constraints for variety of common missile systems. The increased stresses and temperatures result in stronger and tougher materials demands, being met in part by advanced alloys and processing that includes the addition of inoculants [2]. Each system experiences differing temperatures and strains during operations, dependent on the atmospheric conditions, velocities, and maneuvering operations. As new systems are developed, the operating ranges, temperatures, radar absorbing material coatings, and propulsion systems continually evolve. Figure 3 provides estimated temperatures experienced under differing flight conditions. In general, higher velocities increase material temperatures [2] for both external control surfaces and missile skins, and internal structures and propulsion components.

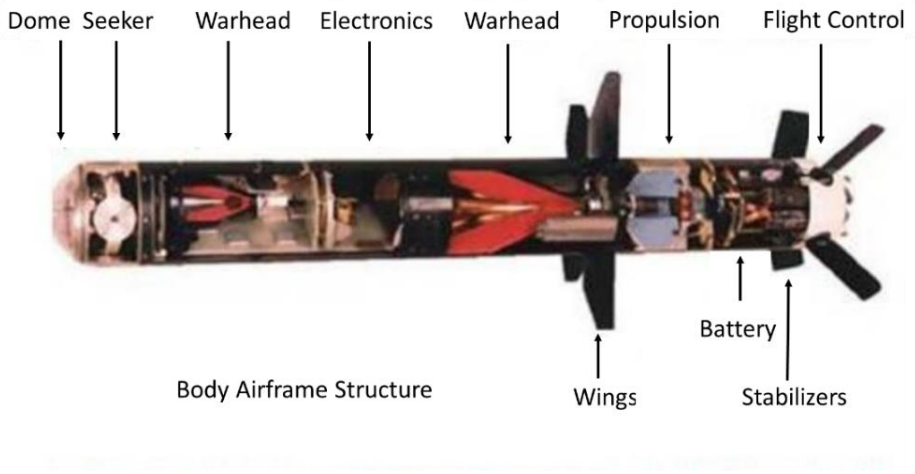

Figure 1: General missile body airframe structure with main components [1].

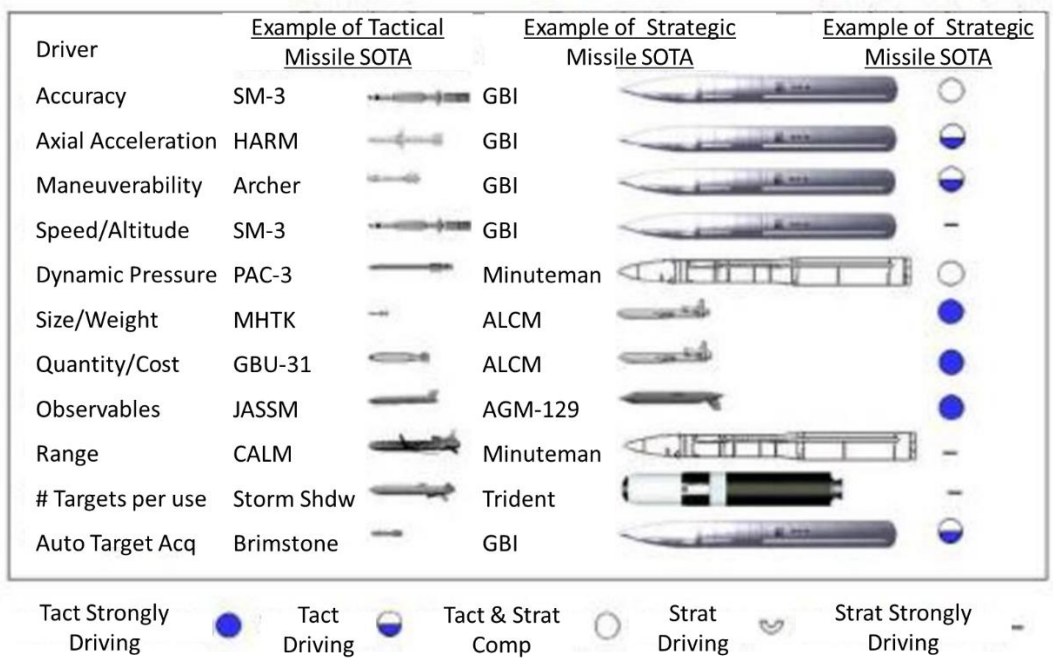

Figure 2: Performance criteria impacting missile design for typical systems [1]

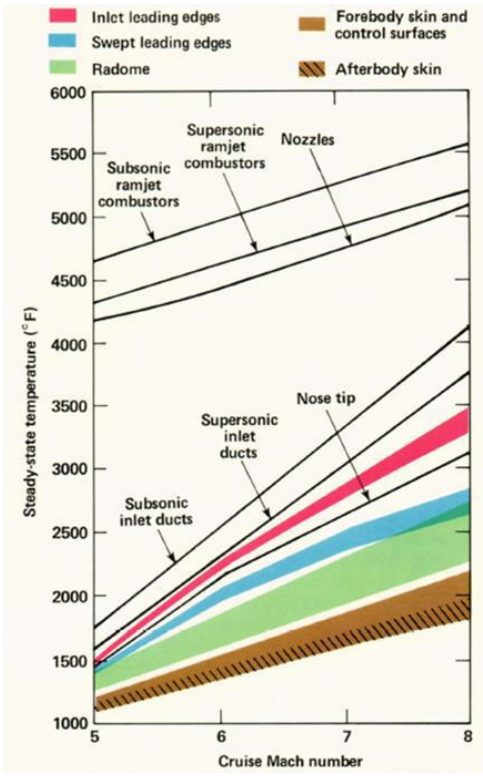

Figure 3: Typical maximum temperatures at 80,000 feet altitude as a function of cruise Mach number for critical components [2].

In general, the materials for these systems can be segregated into four classes: metals, ceramics, polymer, and composites. The plot of Fracture Toughness versus Yield Strength for typical material within these material classes is provided in Figure 4 [3]. In most structural materials, the tensile strength is inversely proportional to the ductility and fracture toughness. As shown in the figure, higher compressive strength materials such as ceramics have relatively lower toughness due to limited ductility. For missile applications, higher temperature environments require design trade-offs between high strength the toughness, as well as ductility and machinability properties required for making specific components. Increased demands for missile maneuverability introduces additional high strains on the airframe and higher operating temperatures which further complicate material selections.

For polymers, environmental conditions typically necessitate the use of high strength fibers and/or additives to create polymer-based composites. The current Missile Technology Control Regime (MTCR) Annex details controls for the four material classes, with emphasis on composites and refractories [4]. For example, composites using resin impregnated fiber preforms having a room temperature specific tensile strength (UTS/specific weight) greater than 7.62 x 104 m and room temperature specific modulus (Young's modulus/specific weight) greater than 3.18 x 106 m (both at 50% relative humidity). However, restrictions are also provided based upon the use of the materials, including the use of pyrolytic fiber reinforced graphite used for rocket nozzles and re-entry vehicle nose tips. Ceramic composite materials usable for radomes are also controlled depending on the dielectric constants.

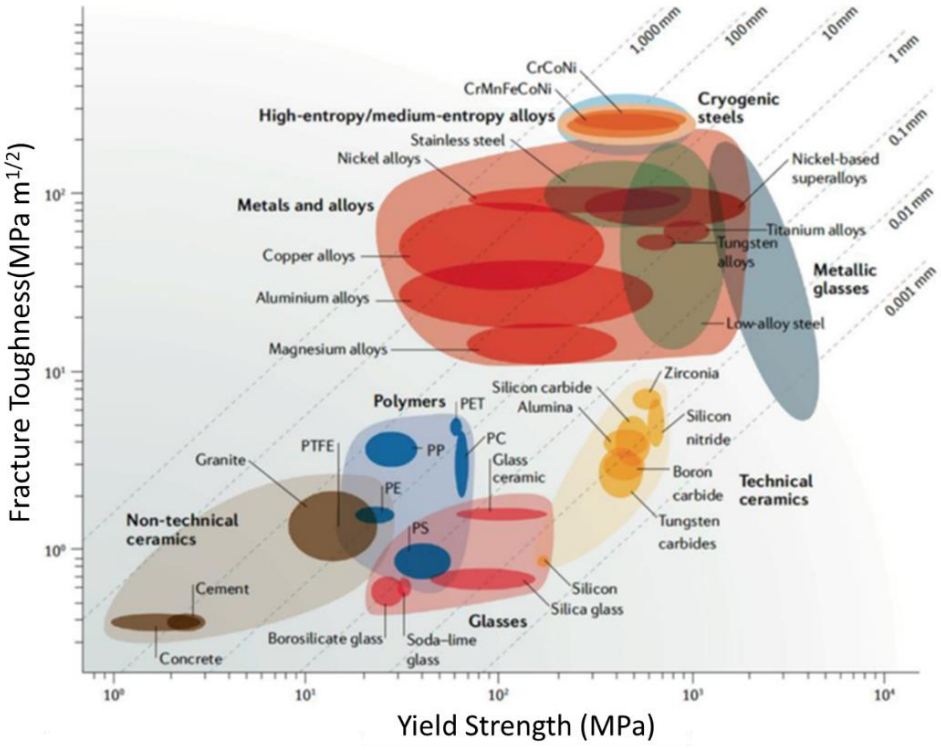

Figure 4: Plot of strength versus fracture toughness of various classes of materials [3].

High temperature ceramics are also addressed, with emphasis on SiC materials used in nose tips, re-entry vehicles, and nozzle flaps (including reinforced SiC composites including C-SiC and SiC/SiC combinations). This applies to bulk ceramic composites that are machinable into components. In particular, the MTCR calls out the use of ultra-high temperature ceramic matrix materials with melting temperatures above 3000C, reinforced with strengthening fibers usable for missile components. This does not apply though to ultra-high temperature ceramic (UHTC) materials in non-composite form. The list of UHTC materials includes Ti, Zr, Nb, Hf, and Ta borides and carbides. These materials are important since they may for precipitates like TiO2 as strengthening agents in complex alloy blends, including high entropy alloys. Ceramic processing sometimes employ inoculant type additions to help wet particles and form binding phases during sintering and Binderjet additive manufacturing.

Metal alloys addressed in the MTCR include (i) W-based alloys in particulate form with W content of 97 wt% or more, and particle sizes of 50 micron or less, and (ii) Mo alloys in particulate form with Mo content of 97 wt% or more, and particle sizes of 50 micron or less. In addition, controls are provided for solid form material compositions with Cu infiltrated W and Ag infiltrated W, (containing 80 wt% or more of W). The main criteria is the ability to be machined into specific geometric shapes (120 mm diameter tubes for example), or blocks of material 120 mm x120mm x 50 mm, or greater. The ability to shape and/or machine the materials plays a significant role in their applicability to missile components. Other controlled high strength alloys include maraging steels and titanium-stabilized duplex stainless steels (Ti-DSS). The constraints on maraging steels target room temperature UTS values equal or greater than 0.9 GPa in solution annealed condition, or 1.5 GPa in precipitation hardened, for specific product forms. Ductility versus Ultimate Tensile Strength (UTS) is shown in Figure 6 for typical steel alloys [5]. Maraging steels are basically steel materials with very low C content that rely on precipitation and solid solution strengthening from non-C element additions (usually Ni). The materials are typically heat treated to age harden the microstructure. Like the constraints on W alloys, the document connects properties to geometric shape, including sheet, plate or tubing with wall/plate thicknesses equal to or less than 5 mm, and tubular forms with a wall thickness equal to or less than 50 mm while having an inner diameter of 270 mm or less. Constraints on Ti-DSS involve those material containing 4.5-7 wt% Ni, 17.0-23% Cr, and 0.10wt% Ti, and a two-phase microstructure with at 10 vol% austenite in specific product forms. The forms include ingots or bars sized 100 mm or larger in any direction, and sheets having a width of 600 mm or more and thickness of 3 mm or less, and tubes have an outer diameter of 600 mm and wall thickness of 3 mm or less.

The MTCR emphasis on strength and machinability stresses the importance of tensile properties and ductility as a function of temperature. Missile service conditions also require addition design considerations including specific weight, corrosion resistance, radiation damage resistance, fracture toughness, fatigue properties, vibration and flight dynamic response, and radar absorbency, among others. In addition, the overall manufacturability and repair of the systems introduces concerns on welding and joining ability, high temperature behavior and stability, reproducibility, machining, and material availability. For example, many of the proposed aerospace materials and components involve critical alloying elements that have limited availability and/or fluctuating costs.

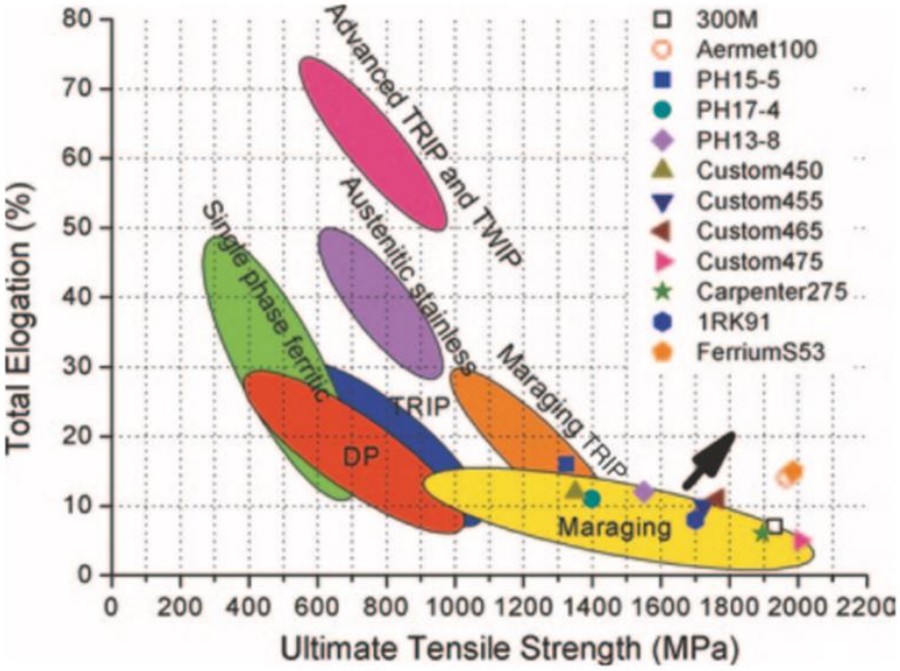

Figure 5: The strength- ductility profile of various steels. The symbols indicate the properties of existing high-end maraging steel grades [5].

The current state-of-art materials for missile designs includes the use of high strength aluminum, maraging steel, and titanium alloys for main support structures. Depending on service mission, carbon-based composites (C/SiC and C/C) are used for nose cones and outer surfaces exposed to high temperatures, as well as for thermal protective and ablative systems (TPS). Refractory alloys including W are used for high temperature regions. Hypersonic and sensing requirements present new considerations (including needs for new sensing window and radome materials). Many of these criteria are competitive and require design trade-offs to optimize overall performance. Strength and ductility are prime examples where increasing material strength traditionally involves decreasing its ductility. However, the growing demand for new missile systems and profiles has encouraged research into providing alternate materials that enhance current performance and overcome current limitations, while reducing overall costs. This document investigates the growing development of inoculants which are added to materials targeting many of these engineering requirements.

Casting is an inexpensive process for producing near net shape components. Unfortunately, the resulting microstructures often have columnar morphologies, grain sizes, and or chemical heterogeneities resulting in lower mechanical properties (compared to wrought products). Inoculants are added to the melt to mitigate casting defects and limitations. They also enable further development of high temperature alloys into near net shapes traditionally produced via casting processes due to limited ductility. These shapes may include the geometric shapes addressed within the MTCR (tubes and limited wall thicknesses). In addition, inoculation provides controlled kinetics and achievable chemical segregation that enables potential for far-from equilibrium thermodynamic microstructures and chemistries that could provide new metastable alloy states and subsequent properties to address co-

design engineering constraints, including needs for increased strength and ductility. An illustration of the inoculant role in solidification is provided in Figure 6 [6].

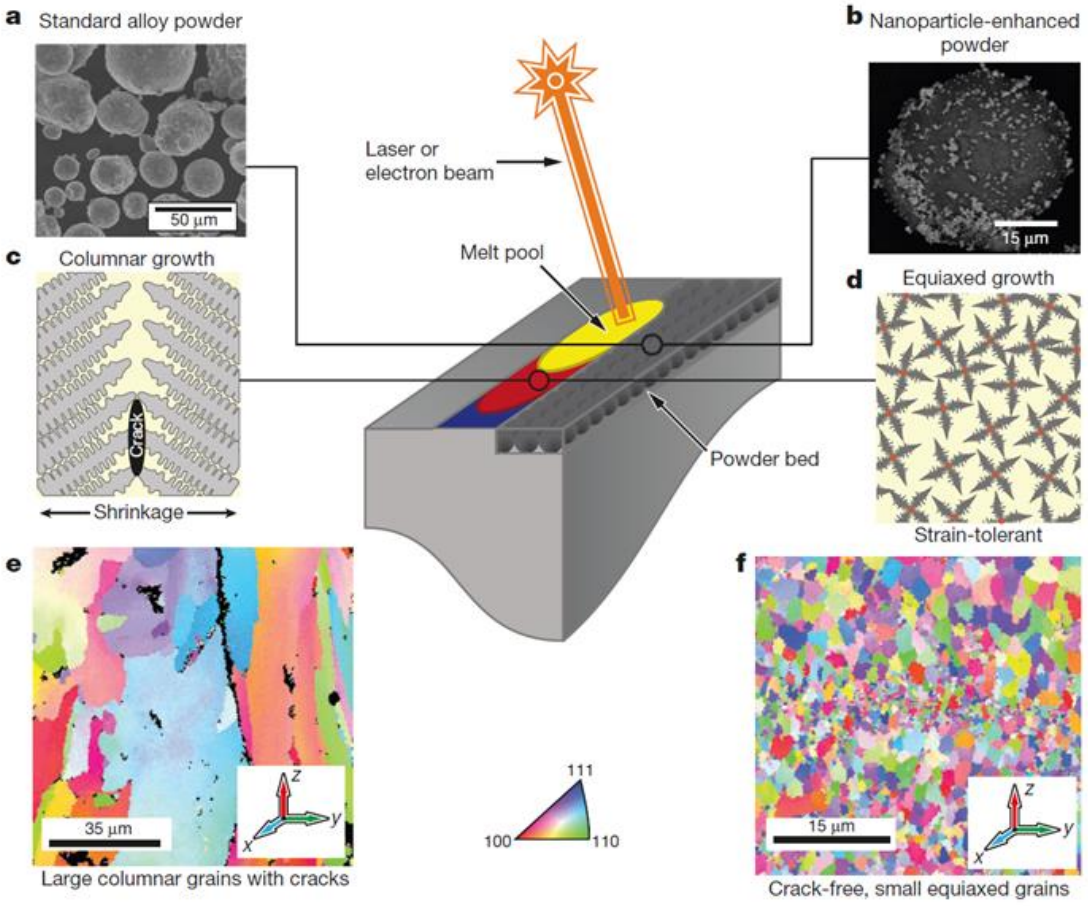

Figure 6: The central schematic represents an overview of the additive manufacturing process, whereby a direct energy source (laser or electron beam) melts a layer of metal powder (yellow), which solidifies (red to blue), fusing it to the previous (underlying) layer of metal (grey).

a, Conventional Al7075 powder feedstock. b, Al7075 powder functionalized with nanoparticles. c, Many alloys including Al7075 tend to solidify by columnar growth of dendrites, resulting in cracks due to solidification shrinkage. d, Suitable nanoparticles can induce heterogeneous nucleation and facilitate equiaxed grain growth, thereby reducing the effect of solidification strain. e, Many alloys exhibit intolerable microstructure with large grains and periodic cracks when 3D-printed using conventional approaches, as illustrated by the inverse pole figure. f, Functionalizing the powder feedstock with nanoparticles produces fine equiaxed grain growth and eliminates hot cracking [6].

Although depicting an additive process, the concept within the melt pool is applicable to the melt environment within castings. The inoculants (and nanoparticles in this example) heterogeneously nucleate the primary equilibrium phases within the melt during cooling. These low energy barrier sites form ahead of the solidification front, creating equiaxed growth that helps reduce strain and prevent cracking during solidification [6]. Figure 7 shows AM powder stock with deposited nanoparticles that act as inoculants during solidification, inducing equiaxed grain growth [6]. Recent research on inoculant use has focused on Al and Steel, with emphasis on additive manufacturing processes. A total of 658

research articles involving inoculant use in alloys were identified over the last 20 years using Web of Science. Of these, 8 of the top 20 cited articles were published in the last 10 years with emphasis on Al and Steel alloys. Additive manufacturing using inoculants was also a key research topic within these articles. This report references the highest 200 cited research articles from this search. General metallurgical information was provided by Askeland and Callister [7, 8]. The five leading materials included steel and cast irons, aluminum, magnesium, titanium, and nickel alloys. For clarification of inoculant terms and casting processes, Al alloys will be addressed first and utilized to convey basic metallurgical principles.

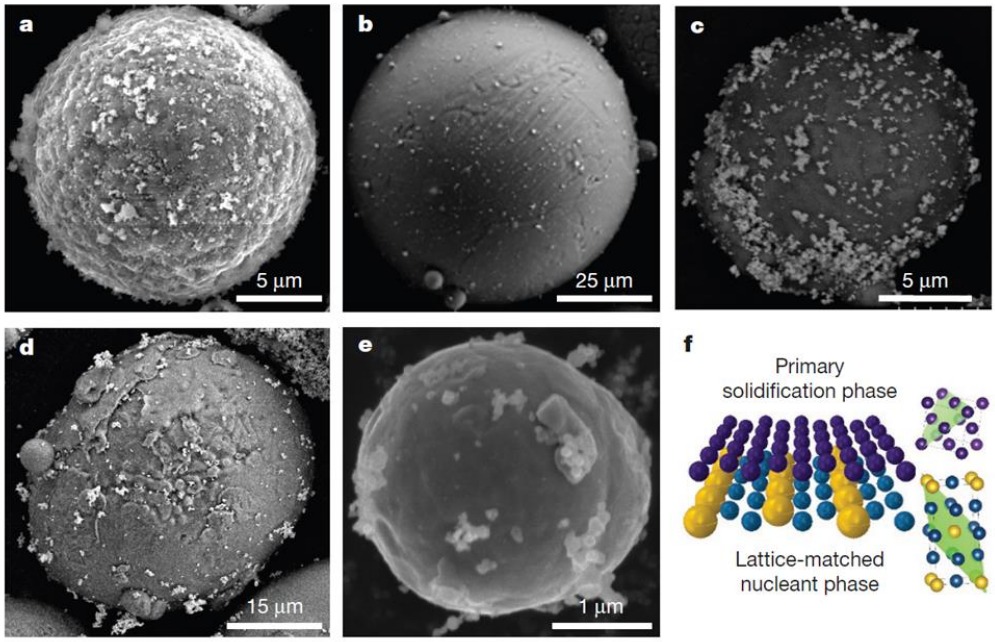

Figure 7: Nanoparticle assembly on additive metal feedstock. The assembly approach enables the production of various feedstocks with different nanoparticle assemblies, which can be target ed to induce equiaxed grain growth a, Al7075 powder with TiB2 nanoparticles.

b, TiAl6V4 powder with ZrH2 nanoparticles. c, Al7075 powder with WC nanoparticles. d, AlSi10Mg powder with WC nanoparticles. e, Iron powder with TiC nanoparticles. f, Schematic representation of how lattice-matched nanoparticles (bottom phase in blue and yellow) can induce low-energy-barrier epitaxial growth of solidifying metals (top phase in purple), with lattice-matched planes in the unit cells indicated in green on the right [6].

2. INOCULATION AND AL ALLOYS

Inoculants have been used in cast Al alloys for many years, primarily for refining grain structures and avoiding casting defects (like hot cracking). The dendritic arm spacing (DAS) influences both ductility and strength, controlled by the cooling rate and not less by alloying [9]. However, grain size is strongly influenced by chemistry, cooling, and mechanical actions that fragment grains [9]. For example, Ultrasonic melt treatment (UST) increased the nucleation potential of $MgAl_2O_4$ particles. The UST process altered the inoculant particles and ultimately increased their number density, which increased the degree of undercooling and led to enhanced refinement of primary Si particles at higher cooling rates [10]. Research on inoculation mechanisms in Al have provided critical insights into the design of Al

castings [9, 11, 12] and predictive models for grain size [13, 14]. These include development of analytical models using phase transformation kinetics to determine the required undercooling and thermodynamic driving forces for specific phase evolutions [15-18]. The incorporation of energy considerations has advanced development of new theories for grain refinement involving nucleation, including the Interdependence Theory, which predicts grain size and assumes grain formation results from the interdependence between nucleation and growth acting together within a local environment controlled by chemistry [16]. Specifically, research involving Gibbs free energy calculations was used to determine phase stability for Al nucleation on Al3Ti and TiB2 interfaces as a function of temperature and concentration [16, 9]. TEM analysis identified TiAl3 as adsorbed layers on TiB2 at lower levels than predicted by equilibrium phase diagrams [9]. This strengthens the case for using B instead of Ti (10-20 ppm B) in the form of Al-5Ti-1B and Al-3Ti-1B rods [9]. Results also report peritectic forming solutes possess a higher nucleation rate in Al alloys than eutectic forming solutes resulting from a higher thermodynamic driving force [17]. The research provides valuable insight and design tools for tailoring Al microstructures across many of the critical Al materials classes. In general, nucleation and refinement are influenced by the rate of solute diffusing through the segregated region within the casting ahead of the solidification front (captured as the growth restricting parameter Q) [9]. Researchers have studied the influence of Q for various alloys, and the impact of Si on poisoning the grain refinement of Ti at Si >3wt% [9]. It should be noted that that the nucleation and growth of grain refinement additives on oxide films can become heavy and sink to the bottom of melts. If the layers are disturbed and mixed into the casting during stirring for example, they can produce significant defects that adversely impact properties [9].

2.1 Pure Al alloys (1xxx series)

Many researchers have studied the impact of inoculants on phase formation and grain refinement using pure Al material. For example, researchers increased the Nb content by 0.10 wt%, reducing the average cast alpha Al dendritic grain diameter from 2000 microns to less than 500 microns. They attributed this to the heterogeneous nucleation of Al3Nb and NbB2 intermetallics. In addition, the inoculants were successful over a wide range of cooling conditions and remelting. Although the mechanical properties were not evaluated, the reductions in grain size are expected to increase strength properties of the alloy [19]. Research involving CeB6 as the inoculant found similar results [20, 21]. Liu, et. al refined pure aluminum from a grain size grade of 870 ± 25 μm to 150 ± 35 μm by addition of 0.4 wt% CeB_6/Al ribbon. Researchers found the grain refining efficacy was improved by controlling the CeB6 particle size. Subsequent research studied the impact of cooling rate on the inoculant efficacy of CeB6/Al in aluminum. At high rates of cooling, the CeB6 particles within the ribbons are reduced to approximately 100nm. Results indicate excellent grain refinement of the inoculant from the combined effect of nano-sized refiner particles and the large undercooling caused by the sudden melting of supersaturated Al-Ce solution [21]. The use of TiC has also been studied [22, 23]. Thermodynamic modeling of the evolution of Al-Ti-C as an inoculant in Al melts has shown in compositions that stabilize TiC in the melt, there is less impact on holding times for inoculant in melt. However, there is substantiate degradation in efficacy when held in compositions that do not stabilize TiC. In similar research, a plasma jet method was employed to create AlN-TiN/Al inoculants which were added to pure Al. Results indicate the refinement efficacy after 60 minutes hold, increasing the tensile, yield, and hardness of the Al alloy [24].

Nitriding was also applied to an Al-5Ti-B melt to obtain AlN-TiN-TiB2/Al inoculants, which were

added to pure Al. The process resulted in refined grain structures increased strength and hardness [25]. Non-traditional materials have also been used as refiners, including Ta to form Al3Ta, and the high entropy alloy AlCoCrFeNiTi to form both Al3Ti and Al3Ni. Ta was shown to reduce the grain size by 1000x. Additions of up to 3% HEA in pure Al changed the microstructure from coarse columnar structures to refined equiaxed grains, with nano-precipitates of Al_3Ti and Al_3Ni. The ultimate tensile strength (UTS) and yield strength (YS) were improved with HEA addition while the elongation decreased. Additions of 3.0 wt.% HEA into the aluminum melt improved the UTS 145.2% from 62 MPa to 152 MPa, and the YS b 173.8% from 42 MPa to 115 MPa. The elongation decreased by 33.3% from 39% to 26%.

Because the processing conditions and size of the inoculant particles play a key role in refining the grain size and influencing microstructure morphology researchers have employed ultrasonic melt treatments (UST) to influence phase formation [26]. In the case of primary intermetallic particles and alpha-Al using pure Al and Al-Zr alloys (Al-0.3Zr-0.1Ti, Al-0.5Zr, Al-0.5Zr-0.5Mg-0.9Si) solidified at various cooling rates of 0.2-70 K s (-1), UST decreased the size and increased both the number density and volume fraction Al3Zr and Al-3(Zr,Ti) particles. Trace elements germanium (0.02 at%), indium (0.02 at%) or tin (0.01 at%) were studied to evaluate precipitation of Al3(Sc,Zr) in a ternary Al-0.06Sc-0.06Zr at% alloy [27]. The inoculated samples demonstrated a 2- to 10-fold decrease in creep rates at 300 °C for stresses above ~18 MPa, but a small reduction in creep threshold stresses from 12 to ~10 MPa compared to the inoculant free alloy with a slightly higher Sc content. germanium

2.2 Al-Cu alloys (2xxx series)

Researchers used Nb and B4C powder to produce Al3Nb-NbB2-NbC/Al inoculant (Al-5Nb-0.75B(4)C) ingots and ribbons, which were used to refine a Al-Cu-Mn alloy [28]. Inoculant ribbons showed modified from dendritic structures to equiaxed crystals and refined the grains, reducing the sizes from 100 mu to 30 mu. In addition, the theta' phases were refined from 83 nm to 40 nm with an increase in number density. Inoculation increased the ultimate tensile strength and elongation of the Al-Cu-Mn alloy from 435 MPa and 8.4% to 514 MPa and 11.5%, respectively. They also reported an increase in weldability with 1% inoculant. X and X studying the refined the coarse primary Si phase of A390 was reduced from 126 to 26 μm by adding 0.7% Al-10Fe-3.2P [29]. The addition also increased UTS 18.2% with a 15.6% increase in Yield (at 720C). Additional research combined Ultrasonic melt treatment and use of Al-3Ti-B master alloy in 7075, 2024 etc. For 2024, with UST and TiB2 grain size reduced to 138um, no UST and TiB2 116 μm [30]. They studied the impact UTS has on grain size in inoculated material. UTS decreased the grain size and inoculate particle size in 7075, 2024, and Al-Cu alloy. Additional researchers inoculated Al-10wt% Cu with A-5Ti-B to develop involving the incorporation globular and dendritic growth kinetics to predict microstructure evolution [31].

Researchers employed powder metallurgy and melt spinning to create AlN-TiC-TiN-Al3Ti/Al inoculation ribbons which were added to an Al-Cu-Mn-Ti matrix alloy assisted by ultrasonic vibration [32]. The subsequent refined structure showed increases in ultimate tensile strength, hardness, and elongation after fracture from 196 MPa, 82.1 HV and 13.6% to 220 MPa, 98.9 HV and 17.4%, respectively. Property improvements were attributed to the AlN, TiN, and TiC nanoparticles within the matrix, and grain refinement. Ram and Mitra, et. al, also studied Ti+B inoculates They used Ti, Ti+B, and Zr in the welding 2090 Al-Li alloy with 2319 and 4043 weld material [33]. All three refined the

grain structure and reduced hot-cracking susceptibility, while increasing post weld hardening response and ductility. Additional study with Ti nanoparticles used as inoculants in SLMed 2024 [34] found 0.7wt% Ti nanoparticles eliminated hot-tearing and columnar structures and provided strength (432MPA) and elongation (10%) properties comparable to wrought samples. Properties were attributed to the formation of Al3Ti particles which are coherent with the Al matrix.

2.3 Al-Si-Mg alloys (4xxx series)

The addition of Si and Mg to Al creates a commercially critical alloy class with many applications (list them). Researchers have modified Al-7Si-0.4Mg +0.25Er with Zr powders to reduce Al dendritic structures and reduce eutectic Si size. Results indicate the addition of 0.6 wt% Zr enabled a morphological evolution of globular dendrites due to the formation of primary Zr containing intermetallics, which increased the mechanical properties [35]. Researchers used an electrostatic self-assembly method to create AlSi10Mg powders homogeneously decorated with TiC nanoparticles. The material was used as an inoculant for SLM processed AlSi10Mg, increasing the UTS from 437 to 456 MPA, and the yield strength 254 to 338 MPA. The microhardness also increased from 113 to 131 HV0.05. Researchers claim the process formed DO22-Al3Ti nanoparticles for the first time using SLM [36]. In similar research, Selective Laser Melted (SLM) AlSi10Mg alloy with (0.2-0.5%) LaB6 inoculant resulted in significant grain refinement attributed to nucleation of Al onto the coherent interface of the LaB6/Al nanoparticles [37]. 10 wt% Al-T-C-B powders added via L-PBF to AlSi10Mg resulted in formation of nanosized B doped TiC particles nucleating alpha Al grains with an average size of 3 microns. Small (30 nm diameter) Si cellular structures also formed, along with 10 nm size Si precipitates distributed uniformly within the alpha Al grains. The resulting material exhibited a high ultimate tensile strength of 488 ± 6 MPa and total elongation of 10.1 ± 2.2%. The enhanced mechanical properties were attributed to the refinement of α–Al grains and Al Si eutectic cells due to the addition of TiC_B inoculants, and particles reinforcement by TiC_B and Si precipitates. The L-PBF approach employed in this research may provide new insights for designing particle contained Al master alloys for 2xxx and 7xxx alloys [38]. Researchers modeled the agglomeration of particles in Al-Nb-B master alloy to determine impact on inoculant efficacy of hypoeutectic Al -Si cast alloys. The model predicts the optimum inoculant diameter sizes and number density during various holding times [39]. Additional inoculants include those containing Fe, P, Cu, C, Ti, and B. Sr and Nb have also been recently reviewed. Adding Na and Strontium to Al with 5-7% Si refines the Si phase from coarse flakes to refined eutectic structure [7]. Although adding Strontium is expensive, it increases ductility. Sodium is less expensive but difficult because of evaporation issues during the process [7]. Researchers studied the effects of adding Al-Fe-P and Al-Cu-P inoculants under differing process conditions on the formation of primary Si particles in cast Al-20Si (wt%) [40]. Inoculation provided uniformly distributed small polyhedral particles in place of the coarse branched Si structures otherwise obtained. The optimized process dramatically increased the number of Si particles and demonstrated the impact of deformation steps and temperatures on the microstructure. Additions of B2O3 and Al2O3 combined with ultrasonic processing increased the grain refinement in A357 (Al-Si alloy), increasing the tensile, yield and elongation values were from 326MPA, 273 MPA, and 6% to 345MPA, 282MPA and 8% respectively [41]. B and Ti additions using Al-3%Ti-1%B inoculants in as cast Al-3%Si and Al-7%Si enabled columnar structures to be refined into equiaxed grains within the small range $0.002 < \%Ti < 0.01$ for Al-3% Si, and of $0.029 < \%Ti < 0.075$ for Al-7% Si. However, larger inoculant additions for the Al-7% Si alloy are attributed to Si poisoning of the inoculant [42]. Low levels of Ti and B in DIN226S (Al-Si-Cu cast alloy), showed that the Ti:B ratio of 1.4 resulted in the highest grain refinement, while a

ratio of 2:1 provided the smallest dendritic arm spacing [43]. The formation of TiC and Al4Sr were studied using the Al-Ti-C-Sr master alloy, which is basically a composite material with TiC and Al4Sr particles within an Al matrix [44]. As an inoculant, the master alloy serves two functions. The TiC refines the Al-7Si alloy by heterogeneously nucleating primary alpha Al, whereas the Al4Sr dissolves into the melt enriching with Sr and modifying eutectic silicon formation during solidification. Similar research to [45], AlCoCrFeNiTi high-entropy alloy (HEA) was added to refine the α-Al and silicon phases in Al-7Si alloy [46]. Fe-rich intermetallics including Al, Si, Co, Fe and Ni, precipitated when the 0.2% HEA was added. The elements of Ti and Cr uniformly distributed within Al-7Si alloy. The additions altered the morphology of the eutectic Si from long needles structure to short rod and granular structures. The inoculant dramatically refined the grains and increased mechanical properties. Multiple researchers have investigated the use of Nb to refine the grain structures in commercial Al-Si castings [47, 48]. This includes research focused on the use of stirring processes during alloy melting to keep NiSi2 from negating the refinement from NbAl3 inoculants [47]. NbB2 and Al3Nb powders were also used as inoculants to refine structures in the commercial alloy LM13 and Al-xSi binary hypereutectic as cast alloys [48]. The Nb and B additions promoted nucleation of primary Al alpha grains and refined the AlSi eutectic phase across the Si additions. For example, the primary Si phase size decreased from 036.6 to 13.9 in the Al-18Si alloy.

2.4 Al-Mg alloys (5xxx series)

A 5083 Al alloy refined with CeB6/Al powder produced a refined grain structure with superior corrosion resistance properties in 3.5% NaCl solution, compared to as-cast and cold rolled alloy [49]. This alloy is used for sea water corrosion properties. Corrosion resistance was evaluated using potentio-dynamic polarization tests. The improvement in corrosion resistance was attributed to the decrease in precipitate formation at grain boundaries. As a novel inoculant, C type fly ash composition and size was investigated for use as an inoculant in AA 5083 alloy [50]. Fly ash materials are by-products of the combustion process in thermal power plants. Specifically, they studied the inoculant impact of fly ash with particle sizes of 40–75 μm, 76–100 μm, and 101–125 μm and weight % of 0.5, 1, 1.5, 2, and 2.5. Strength increased as particle size increased, and as wt% increased up to 2 wt%. However, the strength rapidly decreased at higher levels for all particle sizes, attributed to agglomeration of precipitates and porosity within the material. The elongation value behaved as expected, decreasing for all sized particles as wt% increased from 0.5 to 2%, before increasing. The strongest material corresponded to particle size of 101-125 μm and 2 wt%, with UTS, YS, and elongation values of 400 MPA, 360 MPA, and 1.5%. Similar to the other Al alloys, additions of Al-Ti5B1 and B to alloy 5083 (Al Mg4.5Mn0.7) resulted in modified grain shape and refined weld zone grain size [51]. Additional research on the impact of Sc inoculations in Al alloys [52] found the addition of zirconium intensifies and stabilizes the inoculation action of scandium. Additions of .3 3t%Sc to Al-1.5Mg increased UTS from 120 to 250 MPA, yield from 50 to 160 MPA, and decreased elongation % from 28 to 16.

2.5 Al-Mg-Si alloys (6xxx series)

GTA of Al bead on plate with refiners showed addition of Al-Ti5B inoculant decreased grain size and increased the transition from columnar to equiaxed grains. Materials were 1050A (Al 99.5), 6082 (Al Si1MgMn), and 5083 (Al Mg4.5Mn0.7) [53]. Researchers X and X also added Ti and B to GTA weld material alloy 6082, resulting in grain size reductions from 70 to 21 μm and shifted grains from columnar to equiaxed morphology. The grain refinement further restricted centerline cracking during the

welds [54]. Addition of Ni to Al-Mg-Si (enhanced AA6063) alloy reduced the corrosion rate under 3.65 NaCl solution. The addition of Ni particles created Al2Ni and AlNi2 particles at grain boundaries and increased the formation of Al2Ni3 which reduced corrosion [55]. The alloy A356 is a lightweight and strongly corrosion resistant alloy, often used as a substitute for 6061. Researchers used an ultrasonic mixing technique to prepare SiC, TiC, and Al2O3 nanoparticles for nucleation catalysis in A356 [56]. The researchers investigated the potential impact based on the registry of the catalyst particle and the nucleating material (the alignment of atomic planes on the surface of the nucleant with the planes of the solidifying material). The use of the SiC and TiC nanoparticles reduced undercooling and provided structure refinement although Al2O3 was less successful. The potential use of the nanoparticle inoculants based on registry considerations was recommended to increase refinement and subsequent mechanical properties of the aluminum alloy. Researchers have also used small B additions to refine structures in A356 alloy, transforming columnar structures to equiaxed grains [57], and Sr and Sb modifiers, and Al-Ti-C grain refiners to reduce the Secondary Dendritic Arm Spacing (SDAS) of alpha-Al dendrites and the size/morphology of eutectic silicon [58]. Holding the melt for shorter times modified the eutectic-silicon to a fine fibrous morphology, with a fine lamellar morphology forming at longer melt holding times. By decorating 6061 particles with ZrH2 (1%vol), researchers avoided cracking and columnar grains during laser printing [6]. During melting, nanoparticles of reacted with Al to form Al3ZR, enabling the formation of heterogeneous nucleation sites which resulted in crack free grain sizes of approximately 5 μm (100 times smaller than material without the inoculant).

2.6 Al-Zn alloys (7xxx series)

As with other Al alloys, Ti and B are critical inoculants in Al-Zn alloys. Researchers tested the effect of using a commercial rod versus a ribbon of Al-5Ti-1B as an inoculant in Z22Al (Zn – Al eutectoid alloy) [59]. The ribbon resulted in a more refined Z22Al due to the finer and more uniformly distributed TiB_2 and $L1_2$-Al_3Ti particles formed within the ribbon during its rapid cooling process. The particles acted as heterogenous nucleation sites, increasing the ultimate tensile strength of the alloy from 206 to 230 MPA, and the elongation from 2.28 to 3.01 %. Further adding Zr to the alloy increased the refinement, leading to a 234 MPA UTS and 3.27 % elongation. Nb has also been extensively studied. An addition of 3wt% Nb inoculants to 7075 Al powder altered the microstructure from large columnar grains to refined equiaxed grains and eliminated hot tearing during LPB processing [60]. The resulting 7075-Nb alloy contained a high density of Al3Nb and MgZn2 precipitates. The Mg precipitates formed during the thermal cycling of the LPB. Additional researchers compared using Al3Nb inoculants in SLMed Al-Mg-Zn-Cu alloys [61]. 1.5wt% Nb nanoparticles eliminated cracking and porosity while refining the microstructure into fine equiaxed crystals with size like 1.9um. They claim refinement efficacy is high than in Al3Sc and Al3Ti based on TTT curves, providing a tensile strength of 505 MPA and elongation of 12.3 %. Researchers studied age-hardenable Al7000 series (Al-Zn-Mg) alloys fabricated by selective laser melting (SLM) [62]. Microstructure contained primary Al-3(Sc-x,Zr1-x) particles which acted as inoculants for ultrafine grains, preventing crack formation. The metastable Mg-, Zn-, and Cu-rich icosahedral quasicrystals (I-phase) ubiquitously dispersed inside the grains and aligned along grain boundaries. They reported a yield strength similar to 647 MPA and a ductility similar to 11.6%. Cracking and columnar grain structures in laser printed 7075 were also eliminated using ZrH2 nanoparticles to form Al3Zr. The resulting equiaxed microstructure provided a UTS of 538 MPa with a 3-9% elongation, which is very comparable to wrought 7075 properties, and far exceeds typical AM 7075 values [6].

2.7 Others:

Additional Al alloys have been investigated including TiC additions in Al-B [63] and Al-Pb alloys [64]. The resulting Al-Pb model describes the dissolution of TiC particles and the precipitation of Pb rich droplets in the melt, and the subsequent liquid-liquid phase transformations of the Al-Pb alloy. Researchers demonstrated Al2O3, ZrO2, and TiB2 particles act as heterogeneous nucleation sites for the minority liquid phase in Al-Pb and Al-Bi immiscible alloys. Casting experiments on the alloy Al91Pb9 (wt.%) showed that as the maximum size of the liquid phase droplets decreased with addition of the inoculants [65]. Researchers also tested the refinement efficacy of a commercial Al-3Ti-0.15C grain refiner employed in the twin-roll casting of AA8111 foil stock. Refinement was compared to the Al-5Ti-0.2B master alloy. They reported the critical importance of the process time used to hold the melted materials at temperature.

In summary, a variety of inoculants have been added enhance performance of Al castings. Key improvements, as detailed in Table 1.

Table 1: Key Recent Inoculant Results for Aluminum Alloys

Series/Alloy	Key inoculants	Example Alloy	UTS (MPa)	Elongation (%)
1xxx Al	AlCoCrFeNiTi, TiN	Pure Al + AlCoCrFeNiTi	152	26
2xxx Al-Cu	Sc, CeB6, Ti, B4C	2024+Ti nano Al-Cu-Mn+Nb, B4C	432 514	10 11.5
4xxx Al -Si	B2O3, Al2O3, LaB6	AlSi10Mg+B, TiC	488	10.1
6xxx Al-Si-Mg	Zr, TiC, SiC, Ni	AA6063+Ni	a	a
7xxx Al-Zn	Al3Sc, Al3Zr, Al3Nb, Al3Ti	7000+Al3Scx	647	11.6
5xxx Al-Mg	Fly ash	AA5083+2wt% C fly ash	400	1.5

a: UTS and elongation were not reported, however the corrosion rate of the alloy was decreased.

3. INOCULATION IN STEEL ALLOYS

A short description of steel alloys is needed to clarify terms that describe the relevant microstructure, processes, and alloying features involving inoculants use. The following includes general metallurgical information provided in metallurgical texts [7,8].

Steels refer to iron and carbon alloys. For purposes of clarification, steel alloys and cast iron alloys are typically considered two separate material classes. Classification and specifications for steels are controlled by the Society of Automotive Engineers (SAE), The American Iron and Steel Institute (AISI), and the American Society for Testing and Materials (ASTM), which typically employ a four-digit numbering system. The first 2 digits refer to the element composition and the last 2 refer to the C

concentration. For example, 1010 series alloys refer to a low carbon steel with 0.10 wt% C. In addition, the term hypoeutectic refers to alloys with less than 0.76wt% C. Higher levels refer to hypereutectic steels. Iron alloys typically form multiple phases including ferrite (BCC), austenite (FCC), martensite, cementite, and pearlite (alternating ferrite and cementite layers), depending on the composition and thermal processing. These phases have very different mechanical properties, resulting in the need for controlled alloying and thermal processing to evolve their structures. Elongation and strength properties for steels are plotted in Figure 5 [5], showing the wide variation in properties for these materials.

3.1 *Low Carbon Steels*

The majority of steel production manufactures low carbon steels, which generally contain less than 0.25 wt% C. They usually do not respond to heat treatments intended to create martensite, instead relying on cold work to increase strength [7]. The alloys are weldable, have high ductility and toughness, but relatively low strength. They are typically used in automobile body components, structural shapes including I-beams, and angle irons, and in pipelines, buildings, and bridges [7]. Mn is often included as an alloying element. The alloys have typical properties of 275 MPa yield, tensile strength of 415-550 MPa, and ductility of 25% elongation. Higher strength low alloys (HSLA) are similar but contain additional elements in amounts combining up to 10 wt%. Typical elements include Cu, V, Ni, and Mo. The alloys are heat treatable, increasing their tensile strength above 480 MPa. Examples include A653 and A656 (contain C in 0.22, and 0.18 and Mn in 1.35 and 1.60 wt%) with tensile properties of 520 and 655 MPa, and high ductility of 23 and 15 %, respectively. These alloys are used in truck frames and railway cars, bridges, building support columns, and pressure vessels. Medium C steels have C amounts between 0.25 to 0.60 wt%. Cr, Ni, and Mo are added to improve the ability to heat treat the alloys. The resulting materials are stronger than low C steels, with lower ductility; typically used in gears, crankshafts, and other machine parts [7]. High C steels have C concentrations between 0.60 and 1.4wt%. Tool and die steels are within this class, typically containing Cr, V, W, and Mo. Following hardening and tempering, the materials have the highest strength and hardness of C steels, and lowest ductility. They have high wear resistance and hold sharp cutting edges. They are typically used for knives, blades, springs, and high strength wire. Researchers have studied inoculation in these materials, including the influence of manganese and TiO inoculants on the microstructure in C-Mn steels [66]. They reported that the introduction of >2wt% Mn produced an acicular ferrite dominant microstructure.

3.2 Stainless Steels

Stainless steels have at least 11 wt% Cr as a principal alloying element. They are ideal materials for applications requiring strength and corrosion resistance, which are enhanced by Ni and Mo additions. Stainless steels are further characterized by their dominant microstructure phase, ferrite, austenite, or martensite. Of the three, austenitic stainless steels are the most produced and have the highest corrosion resistance due to higher Cr and Ni additions. They are not magnetic, although ferritic and martensitic steels are. Stainless steels have wide variation in properties. For example, the martensitic stainless steel 440A has a tensile property of 1790 MPa with a 5% ductility in the quench and tempered condition, whereas the ferritic 446 alloy has a strength of 515 MPa and ductility of 275% in annealed condition [7]. Material properties at high pressures and oxidizing temperatures (up to 1000C/1800F) make these alloys potential candidates for missile components and gas turbines. The effectiveness of TiN as an inoculant

in a ferritic stainless steel (AISI 441) processed by laser powder-bed fusion successfully enhanced the microstructures [67]. Ti was introduced during the nitrogen gas atomization of the powders. Adding Ti provided general grain refinement (from 14.2 to 1.2 um) and formed in situ TiN-covered oxide particles (Ti-Al-O) that enabled columnar-to-equiaxed transitions within the melt pool. The presence of O in the feedstock proved advantageous in enabling in situ formation of TiN as grain refiners. Results showed additional composition changes for precipitates within the columnar and fine-grained regions. The same inoculant was employed by researchers investigating the efficacy of up to 1wt% TiN as an inoculant in 304, 316, and 430 stainless steel [68]. Samples were inoculated with FeTi containing 70 wt% titanium, and Cr[Fe]N containing 6.63 wt% nitrogen. In the case of the ferritic stainless steels, including 430, TiN was an effective at refining grains and developing equiaxed structures. For austenitic steels, solidification occurs by the growth of dendritic arms and TiN was not effective at modifying columnar structures. In the ferritic/austenitic steels where ferrite is the leading phase during solidification including 304, TiN is an effective inoculant for refining grains at the 1wt% level. The effects of MgO–Al2O3 oxide and TiN inclusion particles, formed in-situ by addition of Al and Ti in a steel melt, were also studied [69]. Their impact on the formation of equiaxed grains during solidification of Fe-11 mass% Cr-0.5 mass% Si-0.3 mass% Mn ferritic stainless steel was characterized. Results showed the grain size decreased with increasing Ti content, with enhanced columnar to equiaxed transition during solidification. TiN nucleated on the surface of the MgAl2O4 particles due to similar crystal lattice parameters. Impact of Ti inoculant during welding processes have shown excellent results. Researchers modeled the impact of Ti inoculant on grain morphology in Cr-Mo ferritic stainless steel (K44) during gas arc welding [70]. The models predict the size and distribution of Ti forming refractory compounds in the melt pool which act as heterogenous nucleation sites which are used to determine subsequent grain morphologies. Researchers validated the model with bead on plate experiments.

3.3 High Speed and Tool Steels

High speed steels and tools steels have high strength from alloying with W, Mo, Cr, V, and Co alloys to provide materials with elevated hardness and toughness properties, combined with excellent high temperature tolerance. Researchers inoculated AISI M2 high speed steels with powdered up to 0.6wt% W and 0.6wt% WC [71]. The inoculant was added directly into the melt, resulting in refinement of primary grains and creation of a dominant equiaxed grain morphology. Characterization using scanning electron microscopy showed inoculation preferred formation of M6C eutectic at the expense of M2C and MC variants. 0.3wt% W was sufficient to reduce grain size from 65.87 to 35.86 um; increase to 0.6wt% 46.2 um. Inoculation with 0.3wt% WC reduced grain size to 34.27 um. Although the hardness did not significantly change, the toughness improved from 0.05 to > 0.075 MJ/mm^2. Tungsten-molybdenum high-speed steels of AISI M2 and T30 type and low-alloy tungsten-free 1.1C-5Mo-1.7V high-speed steel were inoculated by addition of Bi directly into the melt before pouring [72]. The additions refined the cast structure and morphology of the matrix grains and eutectic carbides. It also redistributed the main alloying elements between solid solution and eutectic carbides. Microstructural changes were attributed to the surface activity of bismuth, which segregates to the liquid/solid interface and restricts dendrite growth in the direction along certain crystallographic planes. The 0.1 wt% addition Bi significantly increased impact toughness of T30 and M2 from values of 0.11 and 0.1 to 0.19 and 0.17 MJ/m^2, respectively. Although the wear resistance was also increased, the hardness of both T30 and M2

slightly decreased in the heat treated and tempered condition from 61 and 58 to 60 and 56 HRC. Bearing steels have also been inoculated to improve properties. For example, Fe-Nb-Cr-C amorphous nanocrystalline inoculants as nanoparticles were also used as inoculants in GCr15 bearing steel, inducing formation of Cr7C3 carbides and grain refinement within the matrix [73]. The inoculant contained 6.5wt%Nb, 0.5wt%Cr, and 93wt% cast iron. Grain size within the bearing steel was reduced from 375.58 μm to 116.45 μm. Hardness increased from 62 to 63.9 HRC, attributed to refinement and reduction of Cr23C6 precipitation in favor of stronger Cr7C3 carbides. Wear rates decreased from 0.0412% to 0.0115%, attributed to the increase in number and homogeneity, and decrease in size of carbides. The yield strength, tensile strength elongation, and reduction of area were increased from, 1786.8 MPa, 1800.9 MPa, 1.12%, and 3.25% to 1970.9 MPa, 2025.7 MPa, 1.85%, and 12.21% respectively.

3.4 Cast Iron

Although the steel alloys described above with lower C levels may be cast during processing, the term "cast iron" typically describes iron alloys with C content above 2.14wt%. At C levels above 6.70 wt%, the compound iron carbide Fe3C (cementite) is formed which effectively limits practical alloying. Typically, the C content is between 3.0 and 4.5 wt%. With the higher C content, these materials are easily melted at temperatures below the melting temperature of steels but have increased brittleness. Casting is used to overcome the brittleness issues which make other fabrication methods difficult. The resulting cementite phase formed in these alloys is metastable and can be decomposed to form C (graphite) and alpha ferrite, dependent on other alloying elements and the cooling rate. Generally, graphite formation is increased by adding Si > 1 wt%, and by slower cooling rates. Similar to steel alloys, cast irons are characterized by phase evolution, forming gray, nodular, white, malleable, and compacted graphite alloys.

Researchers describe a three-stage model for nucleating flake graphite [(Mn, X) S type nuclei] involving three important groups of elements (deoxidizer, Mn/S, and inoculant). They emphasis the control factor (%Mn) x (%S) and ensuring it equals to 0.03 - 0.06, accompanied by 0.005wt.%-0.010wt.% Al and/or Zr content in inoculated irons [74]. They report Fe powder addition promotes austenite dendrite formation in eutectic and slightly eutectic. However, it may have negative influence on the morphology of the (Mn, X) S type graphite nuclei. Adding both iron powder + inoculant appears to be effective for nucleating both austenite and graphite without negatively impacting morphology. Researchers investigated the nucleation of eutectic cells (grains), with the aim of reducing or eliminating carbide formation in thin-wall castings (reducing or preventing chill) [75]. The elements Al, Zr, and Ca introduced into iron by inoculation promoted the formation of complex (Mn,X)S compounds, which featured in efficient flake graphite nucleation with less eutectic undercooling, in agreement with a three-stage graphite nucleation mechanisms. In the first stage, Al and Zr participate an oxide compound formation, while Ca improved the graphite nucleation capability of MnS, which is nucleated on these original oxide sites, in a second stage. The predominant factor controlling cast iron strength is the amount of austenite, rather than secondary dendrite arm spacing. The influence of dendrites on the mechanical properties of gray iron is similar to the reinforced steel bars effect in concrete or fibers in composites acting as a support frame. The greater the dendrite amount, the stronger the cast iron is. The influence of secondary axis spacing on cast iron properties is not as significant as that of the dendrite

amount; nevertheless, with decreased secondary axis spacing, the tensile strength also increased. To create underlay which can increase the rate of crystallization, the mismatch d between lattice parameters of the underlay and inoculated phase should be as low as possible. Researchers have reported that inoculation is most effective when d < 6%, its effectiveness is moderate between 6 and 12%, and it is ineffective if d > 12% [3026]. Titanium carbide (TiC) particles were coated with nickel nitrate (Ni(NO3)(2) and successfully coated onto the surface of a ferrosilicon inoculant [76]. When injected into iron, the inoculants enabled homogeneously dispersed morphological improvement in the crystal phase of the graphite.

3.5 Gray Cast Irons

Gray cast irons have approximately 2.5 to 4.0 wt% C, and 1.0 to 3.0 wt%Si [7]. The graphite exists in the form of flakes, typically surrounded by alpha ferrite or pearlite matrix. The alloys are usually brittle in tension due to the edges of the flakes serving as stress concentration sites. They have higher properties in compression and have excellent vibrational energy damping capabilities, suitable for base structures of heavy machines. The alloys are relatively inexpensive, easily cast, and have low shrinkage, making them candidates for intricate shapes. Researchers adding 0.05wt.% to 0.25 wt.% Ca, Zr, Al-FeSi inoculants into grey cast irons reported that in-mold inoculation has a more significant effect compared to ladle inoculation, especially at lower inoculant usage (less than 0.20 wt.%)[77]. The role of MnS is critical to the graphite formation in these alloys. Eight different alloys compositions with multiple cooling conditions and 0 and 0.5 wt% inoculant (commercial Superseed^{TM}) where evaluated for impact of MnS [78]. Results indicate the inoculants created oxides within the melt that produced MnS nucleation sites. As the nucleation sites increases, the particle size decreased. Additionally, nucleation on the oxides created a stable growth morphology for MnS particles that improved the morphology of graphite. Similar research in grey iron (EN-GJL-200) reported Mn and S contents and the Mn/S ratio respectively play dominant nucleation roles [79]. They also found O did not influence graphite nucleation. Fe powder inoculants were also shown to impact the formation of primary dendrites [80]. Different inoculants have created variety in the microstructures, as shown by researchers [81]. They tested six inoculants having a base of Fe-Si-Ca-Al with additions of Sr, Ba, Zr, Ti, rare earth (RE) and C at different proportions. Two of the inoculants were investigated at three different levels of additions. The results provided different eutectic structures and microstructures. Researchers also employed inoculants to improve thermal conductivity and strength in a pearlitic gray cast iron [82]. Three alloys with similar compositions were inoculated by Zr-FeSi, Sr-FeSi, and SiC inoculants, respectively. The Sr-FeSi provided the highest number of eutectic grains, the highest thermal conductivity, and the highest tensile strength (255 MPa over 230 MPa) in all three alloys. The optimal structure and highest thermal conductivity and tensile strength were obtained by Sr-FeSi inoculant. Others also employed SiC, along with FeSi75, as inoculants in the gray cast iron HT250 [83]. While both inoculants refined the alloy, the one with SiC increased the precipitation temperature of the primary austenite and led to more developed dendrites in the matrix.

3.6 Ductile Cast Irons (DI)

According to Callister [7], adding Mg and/or Ce to the alloy before casting evolves the graphite into

spherical nodules or particles instead of flakes and creating a ductile or nodular iron. In as-cast form, the matrix is typically pearlite. However, the material is often heat treated to convert pearlite to ferrite. Ductile castings are stronger (380 to 480 MPa) with higher ductility (10 to 20%) than gray iron. DI materials are commonly chosen to realize mechanical components and machine parts with structural functions including heavy section wind turbine elements, railway brake discs, crankshaft, wheels, gears, pumps, valves, pipes are only a few examples of industrial applications [84]. Researchers have claimed the alloys provide low cost with the greatest fluidity and the least shrinkage of any ferrous alloys. The applications typically involve cyclic loads and have critical fatigue strength requirements. The microstructure is usually characterized by spheroidal graphite particles dispersed within a metal matrix. The ferritic matrix provides higher ductility and toughness, while the pearlitic provides higher strength [85]. Due to graphite and casting defects, the fatigue strength is lower than many low alloyed steels [84]. Among these defects, chunky graphite is certainly the more frequent. Chunky graphite forms at the thermal center of heavy-section DI and appears macroscopically as black spots in the fracture or saw-cut surface [86]. Researchers studied the impacts of inoculants on formation of chunky graphite using four different alloy combinations of Si, Al, Ba, Ca, Mn, Zr, Bi, and rare earth elements in a cast iron FeSiMg alloy (44–48%Si, 5.75–6.25%Mg, 0–0.80%Al, 1.05–1.45%Ca, 0–0.10%RE, Fe bal., wt%) [86]. The additions provided yield, UTS and elongations of approximately 280 MPA, 385 MPa, and 14%. In-stream inoculation containing Bi and rare earths drastically reduced the formation of chunky graphite. Researchers studied the formation of compacted graphite in FeSiMg casting with 0.10 wt% addition of a commercial inoculants (Si = 69.9, Al = 0.93, Ca = 1.38, Bi = 0.49, RE = 0.37 and Fe balance, wt%) under various cooling rates [87]. Results support the view that a fully compacted structure can be obtained only with a controlled inoculation which must be balanced to avoid too high nodularity. Researchers studying foundry conditions, including inoculation, in 400-18 ductile iron (DI) reported the influence of Mn is depended on the P and residual elements levels [88]. In addition, Si had a significant influence on the mechanical properties of heat treated DI (increasing both yield and UTS while decreasing elongation). For optimum properties, they recommended use of RE-bearing FeSiMg as a powerful inoculant. In their review of heavy ductile iron used in windmill applications, researchers outlined successful inoculant characteristics, including high fading resistance, graphite nodularity recovery and chunky graphite avoidance [89]. For application temperatures less than 1,350 ℃, Sr-FeSi and Ba-FeSi (limited Ca content) systems are usually used. Limited inoculant addition rate is typically 0.15wt.%-0.30wt.%, referring to treated iron. Two groups of active elements are usually associated for this DI application: nodularizing elements (Mg, RE) and anti-nodularizing elements (Sb, Sn, Bi or Pb). They report using rare earth elements as a possible method to balance the contradictory influence of the elements. The effectiveness of 0.4wt% Zr, Sr, and Ba based commercial inoculants was tested in the conventional and ablation casting of ductile cast iron (3C+4.15Si+0.36Mn+0.04Mg+Fe, wt%) [90]. Ablation casting uses water jets to quickly erode the walls of the sand mold immediately after the melt is poured, increasing heat transfer. The inoculant containing 2.5wt% Ba provided the highest nodule count when combined with ablation casting, attributed to the formation of Ba sulfides which acted as nucleation sites. Each inoculant reduced mean graphite diameters with the Ba material increasing yield, UTS, and elongation from approximately 375 MPa, 500 MPa, and 2% to 425 MPa, 550 MPa, and 3.2 %, respectively. Improvements were lower for the other inoculants. Researchers [85] have also used Ce inoculants (75Si+1Ca+1Al+2Ce, and 73Si+1.5Ca+4.5Al+traces of Mg and Ce, wt%) impact on chunky graphite formation EN-GJS-400 ferritic ductile iron. Results show a content of 33% chunky graphite

reduced fatigue limit of ductile iron by 12%, which is equivalent to the reduction in tensile strength. CG was preferential path for fatigue crack propagation, but not proven to be fatigue fracture initiation site. In addition, the higher Ce inoculant provided a reduced UTS and elongation from 412 MPa and 15.9% to 355 MPa and 5.3%., without significant impact on yield. Ce additions have also been used in other DI alloys, including the FeSi DI alloy [91, 92]. For example, the inoculant 0.3 wt.% Ca,Ce,S,O-FeSi alloy [70- 76%Si, 0.75-1.25%Ca, 0.75-1.25%Al, 1.5-2.0%TRE, S and O bearing compounds totaling less than 1%, Fe bal] was an effective inoculant in a FeSi DI alloy to reduce chill and shrink tendency while increasing nodule count in ductile cast iron production. In similar DI work, researchers, successfully produced 3 mm thin wall ductile iron sand castings free of eutectic carbides to compete with Al castings (cost and strength). They employed Bi bearing ferro-silicon as an inoculant, introducing FeSi75 in stream, and Bi bearing FeSi into the pouring basin. The inoculation significantly increased the nodule count in 3 and 10 mm plates. The faster cooling within the 3 mm plate resulted in larger undercooling levels that tripled the nodule count over the 10 mm plate. Increasing the Si content increased the fraction of ferrite, decreasing the strength and increasing the ductility. When three eutectic Fe–C–Si alloys were inoculated with 0.2% (62.6 % Si, 0.22 % Mg, 1.01 % Al, 1.79 % Ca, 5.96 % Mn, 0.13 % Ti, 6.77 % Zr, 0.65 % Ba and less than 0.07 % lanthanides), Ti compounds in carbides and nitrides were found to be major nucleation sites for spheroidal graphite in Fe-C-Si alloys [93].

3.7 White Cast Irons

White cast irons have <1.0wt% Si and rapid cooling rates evolving the C into cementite instead of graphite [7]. Cementite content increases hardness and brittleness, making the materials very difficult to machine and limiting usefulness to hard and wear resistant applications. However, the cementite can be evolved into graphite surrounded by either ferrite or pearlite (depending on cooling rate). This creates malleable iron, which has high strength and improved ductility. Applications of the malleable iron include connecting rods, transmission gears, flanges, pipe fittings, and valve parts. Researchers investigating inoculant impact on graphite nucleation in white cast irons reported an increase in the amount of SiCaMn from 0.5 to 0.8 kg/T increased the fraction of precipitated graphite without impacting the count number [94]. The addition of 1 kg/T of FeTi, affected the graphite morphology, developing elongated graphite shapes without modifying the amount of graphite. Studies involving 1-3wt% TiBAl inoculant additions to hypereutectic high chromium white cast irons improved microstructures and notch toughness [95]. Results show inoculation of 1 wt.% reduced the sizes of the primary carbides while the sizes of the secondary carbides increased and formed in hexagonal form similar to the primary carbide (but in smaller size). Inoculation of 2wt% increased impact toughness properties.

Researchers inoculated Fe-30.5 % Mn-7.55 % Al-0.76 % Si-1.11 % C-0.51 % Mo steel with 0.05 and 0.1 wt% Ce, adding it either into the tap, or in-mold [96]. Although addition of 0.05 % Ce during the tap slightly reduced grain size, the in-mold inoculation with 0.1 % Ce produced an order of magnitude reduction in the grain, from 10-12 mm to an average of 100 mu m.
Inclusions in the 0.05 % Ce steel were mainly cerium sulfides while inclusions in the 0.1 % Ce steel were mainly complex cerium oxides, sulfides, and phosphides. Inoculation greatly increased the nonmetallic inclusion density from 183 to 571 inclusions/mm(2) decreased the solution-treated notch

toughness from 295 to 141 J. In the as-cast condition and for steels aged for 10 h at 530 degrees C, toughness slightly increased with 0.05 % Ce addition, attributed to cerium removal of phosphorus from the melt during solidification. However, toughness decreased with increasing volume fraction of inclusions and decreasing inclusion spacing regardless of the grain refining effect. Because Ce is very reactive in the melt and readily combines with sulfur and oxygen as well as any residual phosphorus, sulfur and phosphorus must be eliminated from the melt to avoid forming Ce sulfides and complex phosphides. The researchers suggest additional Ca for desulfurization prior to Ce inoculation, and the use of nonphosphate bonded refractories to eliminate phosphorus. The effect Mg-Al, Mg-Ti, Al-Ti, and Ce-Al, on the quench solidification structure of Fe-2 wt%Ni-1 wt% Mn-1 wt% Mo alloy was also tested [97]. They were simulating cooling conditions during welding processes, reporting Mg-Ti enabled formation of MgO(MgAl2O4)-TiN complex compounds resulting in fine equiaxed crystals. At longer holding times at higher temperatures, the larger fraction of Ti2O3 and very fine TiN resulting in poor equiaxed crystals. Mg-Al created initially columnar structures. However, the fraction of MgAl2O4 spinel increased during longer hold times resulting in the formation of fine equiaxed crystals. In addition, Ce-Al provided a small portion of equiaxed crystals, and Ti-Al produced the fewest equiaxed crystals due to the formation of alumina.

Castings made of chromium cast iron are generally applied for hostile conditions, where intense wear is the main problem [98], including mining and mineral processing. Researchers typically try to increase wear resistance and strength in these alloys while maintaining low cost compared to Cr alloys. However, adding additional elements to increase alloy strength can be expensive. Inoculants are a possibility since they modify structure while using low element additions to the alloy. Researchers focused on heterogeneous inoculation with both (ferrotitanium (FeTi67) and mischmetal (consisting mainly 67% Ce and 33% La). They used a W0 eutectic chromium cast iron for the base and added both inoculants at 0.06wt% each, and at 2wt% each. In both cases, the inoculants reduced average carbide area by > 19% and increased hardness by over 50%. The wear resistance was also dramatically improved. Results indicate TiC and Ce2O2S work as an effective nucleus for crystallization of Cr7C3 carbides. Ti inoculants were also tested with a hypereutectic high chromium cast iron. Up to 6wt% Ti was added to Fe-25wt%Cr-4wt%C) to test microstructure evolution [99]. Ingot samples were prepared using in an arc furnace by melting pieces of the cast iron with titanium powder. Ti did not act as an inoculant to reduce the size of coarse primary carbides. However, increasing Ti enabled the formation of TiC and depletion C from the alloy, modifying the alloy from a hypereutectic to hypoeutectic microstructure. The finest microstructure was achieved with 2 wt.% Ti, enabling a eutectic structure with mixed chromium carbides and titanium carbides. With additions of 6 wt.% Ti, the microhardness of the primary austenite phase was increased from 268 HV to 342 $HV_{100\,mN}$, higher than 268 HV in the hypoeutectic sample. Although the microhardness of the austenite increased at Ti levels above 2 wt%, the microhardness results indicate hardness increases from 58 to 64 HRC and increased wear resistance for additions only up to 2 wt%. Both hardness and wear resistance decreased at higher levels. Researchers reported the addition of 0.5 wt pct LaB6 led to a reduction of the average grain size from 765 to 92 μm and the proportion of the columnar structure from 35 to 8 pct in an as-cast Fe-4Si ferritic alloy. LaB6 decomposed within the melt, with La and B reacting with Fe, O and S, to form different compounds. Researchers identified La2SO2 and La2O3 particles within the ferrite grains and Fe2B along the grain boundaries, creating enhanced heterogeneous nucleation of d-ferrite by La2SO2, and the

solute effect of B. Researchers have modeled the roles of TiO and AlN as inoculants in steel using thermodynamics. They concluded the metallic TiO behaves differently in the materials, leading to increased nucleation and formation of equiaxed fine grain structure in solidification [100]. However, AlN induces inequalities in the grain structure, forming textures and abnormal grains during annealing. This behavior is attribute to AlN precipitating anisotropically on the (111) plane along the [110] direction of bcc Fe. This assists in the selective growth of specific grains and promotes specific texture, leading to abnormal grain growth. Researchers also studied the influence of cooling rate on V(C,N) precipitates that act as inoculant particles promoting proeuctectic ferrite nucleation in continuous cast low carbon steel (YQ450NQR1) (C 0.12, Si 0.45, Mn 1.26, P 0.02, S 0.01, V 0.12, N 0.013, Fe bal, wt%) [101]. Researchers have also added (0.014wt%) Ti and (0.025wt%) Nb as inoculants directly onto continuously cast slab surfaces to evolve surface microstructure and second-phase precipitation behavior [102]. Carbonitrides of the microalloying elements promoted the nucleation of proeutectoid ferrite castings. The addition of 0-0.25 wt.% Ca, Al, Zr-FeSi inoculant a hypereutectic and a hypoeutectic alloy, both with low S and Al. In the slightly hypereutectic iron, inoculation refined the structure, promoting high eutectic cell count. This favored evolution of graphite morphologies and increased pearlite [103]. Investigators determined O is not desirable when commercial and pure Ca inoculants are used in cast irons, resulting inferior mechanical strength, with increasing chilling susceptibility [104]. They attribute this to reduction in CaC2 formation. Relatively large contents of oxygen in the inoculated melt led to a reduced cell count. SiC particles were added to the molten pool of a high strength low alloy steel (ER110S-G) during WAAM, resulting in grain refinement and the precipitation of Fe3C due to SiC dissociation [105]. The additions improved yield, UTS, and elongation from 681 MPa, 870 MPa, and 39% to 876 MPa, 1070 MPa, and 23%, attributed to the refined grain structures and the dispersed Fe3C particles. Researchers used three inoculants (Si-Al-Ca-Ce+S, Si-Al-Ca-Ce+La, and Si-Al-Ca) to nucleate lamellar graphite cast iron [106]. Graphite was found nucleating at the center of MnS particles. The inoculants did not have a strong impact on the microstructures. Treating the materials with Mg could also result in MnSMg particles within the matrix and graphite centers. Three additional inoculants (FeSi75%, FeSiCaBa, and FeSiMg) were used in cast iron (Fe 1.6Si 0.2Mn 3.8C) with a SiMgMn nodulizing alloy [107]. FeSi75% and FeSiCaBa increased the austenite precipitation temperature, increasing the dendrites in the gray iron matrix and reducing both graphite size and microporosities. FeSi75% also provided the lowest number of nodules and the lowest elongation. The three inoculants had relatively similar UTS values of approximately 515 MPa. Researchers studied the effects of S content on MnS precipitation with several kinds of oxide nuclei [108]. The found MnS precipitation on oxide particles depended on S content. When S content was below 100 ppm, only select oxides served as nucleation site. It was more effective to use an oxide having high sulphide capacity and low melting temperature for uniform dispersion of fine MnS. However, when S was above 100 ppm, almost all the tested oxides served as the precipitation sites of MnS. In that case, it is better to select the oxide which tends to disperse finely itself in steel. Similar research on low carbon steels reported the distribution of MnS became uniform by the complex deoxidation with Mn-Si-Zr, of which complex oxides dispersed finely [109].

Researchers have also added (0.014wt%) Ti and (0.025wt%) Nb as inoculants directly onto continuously cast slab surfaces to evolve surface microstructure and second-phase precipitation behavior [110]. Carbonitrides of the microalloying elements promoted the nucleation of proeutectoid ferrite castings.

The addition of 0-0.25 wt.% Ca, Al, Zr-FeSi inoculant a hypereutectic and a hypoeutectic alloy, both with low S and Al. In the slightly hypereutectic iron, inoculation refined the structure, promoting high eutectic cell count. This favored evolution of graphite morphologies and increased pearlite [111]. Investigators determined O is not desirable when commercial and pure Ca inoculants are used in cast irons, resulting inferior mechanical strength, with increasing chilling susceptibility [112]. They attribute this to reduction in CaC2 formation. Relatively large contents of oxygen in the inoculated melt led to a reduced cell count.

3.8 Compacted Graphite Iron

In these iron castings, C exists as graphite promoted by Si (between 1.7 to 3wt%). C is normally between 3.1 to 4.0wt% [7]. The microstructure contains graphite with a vermicular (or worm-like) shape and limited nodules (less than 20%). Mg and Ce are often added in lower amounts than in ductile iron. The combination of limiting nodule formation and graphite flakes while preferentially evolving vermicular structures requires complex alloying and processing. Increasing nodularity increases strength the ductility. Ferritic matrices have lower strength, but improved ductility than austenitic ones. Typical strength properties are comparable to ductile and malleable irons, with ductility between gray irons and ductile irons. However, the alloys have higher thermal conductivity and resistance to thermal shock [7]. Applications include engine blocks, exhaust manifolds, gearbox housings, flywheels, and brake discs for high-speed trains. Researchers studied the influence of nonmetallic inclusions as nucleation sites for compacted graphite, and impact of trace Ce, Ti, and Zr elements [113]. FeSiMg alloys with multiple trace elements were inoculated with 0.2% commercial inoculants, one with higher Ce (High Ce, low Mn and Zr) and one with high Mn and Zr (low Ce, High Mn and Zr). In the low Ti alloy, (MgSiAl)N and not Ti(CN) acted as nuclei for graphite formation. In the high Ti alloy, sulfides and Ti(CN) were the nuclei. No Mg(MgSiAl)N were detected, due to the N reacting primarily with the Ti. MgO and (MgAl)O acted as nucleation sites for sulfides. Researchers used phase field simulations and experimentation to study solidification in the cast iron EN-GJL-200 with and without inoculants [114]. Results showed that different oxygen contents had little influence on the nucleation in cast iron melts. MnS precipitates were identified as the preferred site for graphite nucleation.

3.9 Steel and Cast Iron Summary

Many different inoculants have been recently applied to improve the castability and properties of steel and iron castings. In addition, new casting processes which include steps to fragment grains and evenly disperse elements and precipitates have resulted in improved castings. A subset of the inoculants and their impacts are summarized in Table 2.

Table 2: Select Inoculants used in Recent Casting Research

Alloy Type	Inoculants	Example Alloy	Inoculant/Property Impact
Bearing Steel	Cr7C3	GCr15+Cr7C3	UTS 2025MPA, 1.85%El, wear rate 0.01%
High Speed Steel	Bi, W, WC	T30+Bi M2+WC	Inc. toughness 90% to 0.19MJ/mm2 Inc. toughness 50% to 0.075 MJ/mm2

Stainless Steel	TiN, FeTi, MgAl2O3	AISI441+TiN	Grain refinement, equiaxed grains
Gray Cast Iron	SiC, FeSi75, (Zr/Sr)-FeSi	HT250+SiC	Refined grains, developed improved dendrite structures
Ductile Cast Iron	Ca, Mn, Zr, Ba	FeSiMgC+Ca,Mn,Zr FeSiMnMgC+Ba	UTS 385 MPa, Elong 14% UTS 550 MPa, Elong 3.2%
White Cast Iron	Ce, La, SiC, Ca, Zr-FeSi SiC, Fe3C	W0 Eutectic Cr+FeTi ER110S-G+Fe3C	Inc. hardness 50%, imp wear resistance UTS 876 MPa, Elong 23%
Compacted Graphite Iron	Ce, Mn, Zr	FeSiMg+Ce,Mn,Zr	Improved graphite formation

4.0 INOCULATION IN NI ALLOYS

Nickel alloys are extremely strong materials, often used in oxidizing high temperature and or radiation environments for extended time [7]. Many aerospace and nuclear nickel alloys rely on precipitation strengthening through alloying with Al, Ti, Co, Cr Mo, and W. Although they have relatively high densities, they are used in missile applications. Researchers used eutectic WC-W2C inoculants during the selective laser melting (SLM) of IN718 [115]. As with other applications, the inoculants provided heterogeneous nucleation sites for grain formation. In similar research, IN718 powder was blended with 0.2 wt. % of CoAl2O4 particles during an SLM process, reacting to form a dispersion of Al-rich nano-oxide particles in the matrix [116]. The inoculants facilitated the formation of fine, equiaxed grains and reduced the degree of crystallographic texture. In addition, the nano-oxide particles restricted grain boundary mobility during heat-treatment and promoted a refined bimodal grain structure. Elastic anisotropy was greatly minimized by the reduction of crystallographic texture. Creep testing at 650 degrees C/650 MPa revealed a reduction of strain rate from 8.8 x 10(-9) s(-1) to 4.9 x 10(-9) s(-1), and an increased creep rupture life extension by 52 hours. Mixing Co3FeNb2 and CrFeNb inoculants refined the gamma matrix grains in IN718C [117]. The addition into the melt also reduced the subsequent shrinkage porosity and increased the formation of equiaxed grains. IN100 is also a common alloy used for high temperature, high strength applications. Inoculation under applied fields was investigated to determine efficacy of CoAl2O4 in IN100 [118]. Under reversible electromagnetic stirring, inoculation refined the average equiaxed grain size of IN100 to 95 mu m and increased the fraction of equiaxed grains to 100%. IN713C castings were also modified by adding 5 and 10 wt% CoAl2O4 inoculant to the prime coat of the shell mold, which react with alloying elements (e.g., Cr, C, Ti, and Al) to form Co particles on the surface [119]. The particles acted as nucleation sites for the heterogeneous crystallization. The alloy matrix consisted of gamma Ni phase strengthened by cubic, coherent precipitates of gamma'-Ni3(AlTi) phase. The interdendritic areas revealed the presence of NbC primary carbides, as well as that of gamma + NbC, gamma + gamma' and gamma + Ni7Zr2 + M3B2. Direct pouring of CoAl2O4 inoculants (5wt%) under the controlled melt-pouring temperature at 1520C also increased mechanical properties in IN713C investment castings [120]. Yield stress and elongation was increased from the handbook values of 689.5 MPa (100 psi) and elongation A4 min. 3%, to 815 MPa and elongation to 7.65% at ambient temperature. However, the modified alloys had significant reduced times to rupture (from 76.8 hours to 7.4 hours). Researchers also reported the formation of microcracks in large eutectic gamma', carbides and borides, during tensile testing, which were attributed to the accumulation of stress at the matrix interface. Inoculation with additions of Ni Al, Ni2Al3, ZrC, NbC and B in investment cast IN 738LC, at temperatures slightly above the liquidus, refined the microstructure and formed equiaxed grains [121]. Researchers attributed grain refinement to surviving active nucleants (undissolved carbide particles and/or inoculants added) which served as nucleation sites

for gamma-crystallites. Specifically, the combination of inoculating the melt with Ni2Al3 under controlled cooling considerably enhanced the grain refining effect.

Superalloys 718 and IN100 are important aerospace alloys with improved properties through additions of WC and CoAl2O4 inoculants. Zr, Cr, CoFeNb, and CrFeNb inoculants have also been used in Ni alloys. Although the additions improved some properties, they reduced others, and in limited cases, created microcracks within the materials.

5.0 INOCULATION IN TI ALLOYS

Wrought Ti alloys are typically very strong (>1400 MPa) with low densities and high ductility (>10%) [7]. However, they are extremely chemically active with other elements at elevated temperatures, sharing a strong affinity with O. Although relatively expensive in comparison with steel and aluminum castings, their corrosive resistance properties and strength make them excellent candidates for aerospace and marine applications, surgical implants, and chemical applications. Specifically, Ti alloys are used in missile propulsion applications and support structures. There are multiple references to Ti materials in the MTCR. As-cast properties are usually lower than wrought due to microstructures. However, additive manufacturing and advanced processing has targeted improving near net shape properties through controlled melt pool geometries and deposition techniques. This may include the addition of inoculants to impact phase evolution during solidification. Given their critical use within multiple industries, it is not surprising that researchers have developed models to predict the impact of inoculants on the phase evolution and mechanical properties of cast Ti alloys. For example, phase field modeling was used to demonstrate the impact of inoculants on the formation of equiaxed polycrystalline structures in Ti-6Al-4V during SLM [122]. The model predicts use of inoculants to create equiaxed polycrystalline structures instead of columnar grains. In reference to inoculants, TiN and ZrN were studied as grain refining inoculants in Ti-6Al-4V using a Wire Arc Additive Manufacturing process [123]. The TiN particle additions reduced the beta grain size and modified them from columnar to equiaxed grains with an average size of 300 mu m. The ZrN powder was not effective at the low levels studied. Additional research involving this alloy used a vacuum rapid solidification technique to prepare in situ Ti5Si3/Ti composite ribbons [124]. The ribbons were used as inoculants in Ti-6Al-4V to obtain titanium matrix composites (TMCs). The addition of 0.6wt% Ti5Si3/Ti refined the TMC grains from 650 mu m to about 110 mu m and acted as strengthening particles to improve the mechanical properties. In similar research, the vacuum rapid solidification technique was used to prepare TiB+TiN/Ti inoculants ribbons. The ribbons were added to TC4 alloy melt to form refined TMCs. The subsequent grain refinement and phase evolution increased the ultimate tensile stress 14.8% to 1070 MPa with 6.68% plastic strain. However, the elongation decreased by 17.3%. The fracture strength increased as volume fraction of reinforcements increased before reaching a maximum at 0.75 vol%.

Isomorphic self-inoculation models for grain refinement of a Ti-Al alloy [125] were used to test Ti-10Al-25Nb as an inoculant ally for a beta solidifying Ti-46 alloy. Isomorphic self-inoculation involves using inoculates with the same crystal and composition structure as the parent phase, resulting in phase evolution through epitaxial growth instead of classical nucleation mechanisms. Results indicate the number of inoculants, and not the particle size distribution, impacted the final grain size. Processing specific Ti alloys can be difficult due to intrinsic brittleness and limited slip mechanisms, including TiAl which has introduced as a high temperature, light weight aerospace material. Additive manufacturing provides potential for manufacturing TiAl, but only if the alloy survives the high thermal stresses

generated during rapid cooling. Researchers used 0.5 wt% LaB6 nanoparticles (100 nm dia.) as inoculants for LAM gamma TiAl, reducing the grain size of the as-printed alloy from 39.81 mu m to 1.5 mu m through 0.5 wt% LaB6 addition [126]. Inoculation also transformed the microstructure from coarse near-lamellar colonies into equiaxed and fine grains, increasing the compressive yield strength, ultimate strength and strain to fracture from 842.9 MPa, 1806.9 MPa and 11.5% to 1089.3 MPa, 2031.6 MPa and 18.6%, which are 29%, 12.4% and 61.9%. Additional alloys have been studied, including reinforcement of Ti-48Al-6Nb by the addition of AlMo/B4C inoculant powders [127]. The inoculants refined the grain size and lamellar width of the alloy. Compressive properties and 3-point bend test results were attributed to the strengthening and toughening mechanisms induced by dual-scaled Ti2AlC and Mo2B5. The ultimate compressive strength and strain at room temperature improved from 1421 MPa, 13.23% to 2276 MPa, 19.22%. The ultimate compressive strength and strain in 1073 K are improved from 758 MPa, 20.05% to 963 MPa, 34.00%. The average ultimate RT strain and strength increased from 3.42% and 1433 MPa to 19.03% and 2195 MPa. The average ultimate 1073 K strain and strength improved from 19.98% and 763 MPa to 33.14 % and 938 MPa. Alloys Ti–44Al–5Nb–2Cr–1.5Zr–0.4B– 0.07La and Ti–44Al–5Nb–1Cr–1.5Zr–1B–0.17La (at%) were also created using an electron beam casting technique and inoculated with LaB6 [128]. Increasing B content from inoculation increased refinement of the microstructure, resulting in a mean structural grain size of 30 μm with 12.8 μm standard deviation. Researchers report LaB6 re-precipitated into complex boride particles, acting as randomly distributed seeds that promoted refinement. Advanced characterization showed the origin of structure refinement consists in solid-phase germination of alpha(2)-Ti3Al-phase on (Ti,Nb)B ribbon-like colonies with subsequent growth of alpha(2)-laths through the gamma-TiAl matrix. The use of Hf5Si3 particles as inoculants in a Ti-2Si-2Nb-2Fe-1Hf-1Ta-1W alloy also increased mechanical properties [129]. The particles provided sites for the nucleation of Ti5Si3, which led to the formation of (TiHf)(5)Si-3 compound phase. The homogenous distribution of (TiHf)(5)Si-3 precipitates hinder alpha grain growth and the movement of the activated dislocations, providing a high tensive strength (942 MPa) with a high level of plasticity (14%).

Given application demand for Ti-6Al-4V and gamma TiAl, it is not surprising that these alloys have been the main focus of Ti alloy inoculation to date. The leading inoculants have been TiN, TiB, TiS, and LaB6, which impact properties through grain/lath refinement, and phase evolution. Although the use of inoculants has increased the cast tensile properties above 1000 MPa with elongation >6% in limited TMCs, improvements must be balanced across multiple properties, including impacts on toughness, weldability, ductility etc.

6. INOCULATION IN MG ALLOYS

The use of Mg alloys as light weight structural materials are increasing. It is limited by cost, strength, and corrosion properties when compared to Al and steel. However, the use of inoculants provides increased strength through grain refinement and particle strengthening while increasing corrosion resistance. AZ91D is the most widely used magnesium die cast alloy. It has excellent mechanical strength, castability, and corrosion resistance.

Researchers have investigated the use of differing inoculants for both casting and welding processes. The addition of SiC inoculants in AZ91 refined grains and formed the Mg2Si phase with script-like morphology [130]. Following solution treatment, Mg2Si phase developed a particulate-shaped morphology with smooth boundaries, increasing the maximum tensile strength to167 MPa. The same

alloy was studied in reference to pure C powder blown into the superheat treatment using a carrier gas [131]. The process created Al4C3 nucleants within the alloy. In similar research involving AZ91, researchers employed 1 μm size Al2O3 inoculation particles at 1 wt% using a mechanical impeller, followed by sonication [132]. The addition of the particles reduced the average grain diameter of AZ91E from 202 μm to 79 μm. The combination of particles and sonication further decreased the size to 54 μm. Although sonicating the material without inoculants also decreased the average grain size, the use of the inoculant proceeded a more uniform and equiaxed microstructure with and without sonication. The addition of 1 wt % Al2O3, increased the UTS, YS and elongation from 138 ± 2 MPa, 95 ± 2 MPa and 1.4 ± 0.1%, to 152 ± 0.5 MPa, 106 ± 3 MPa and 1.6 ± 0.1%, respectively. Further enhancement was achieved through combined UTS and inoculation, increasing the UTS, yield and elongation properties to 163 ± 1 MPa, 113 ± 2 MPa and 2.1 ± 0.1, respectively. The UTS provided significant improvement in ductility. Ti has also been used as an inoculate in AZ91 [133]. The addition of Ti inoculants promoted the nucleation of alpha-Mg grains and the formation of equiaxed dendritic grains during resistance spot welding of AZ91. The inoculate increased the weld shear strength by approximately 10% and ductility by 25%.

Addition of 0.08 wt% Ca into AZ31 melts formed Al2Ca intermetallic compounds that reduced the average grain size of thin strips produced by twin-roll-cast from 100 μm to 30 μm [134]. Researchers validated a simulation method for heterogeneous nucleation based on a free growth model using SiC powders to refine grains within AZ31 under differing cooling rates [135]. The model accurately predicted grain size as a function of the particle size distribution, the volumetric content of ceramic inoculants, and the cooling rate. Additions of >0.04 wt% SiC resulted in significant grain refinement from >120 μm to <50 μm for cooling rates above 3K/s, and enabled formation of an equiaxed microstructure. Researchers have also used phase field models to predict inoculation impact in AZ31 [136]. Phase-field models characterized the columnar-to-equiaxed transition present in magnesium AZ31 alloy solidified under five different welding conditions, including the impact of Ti, Al8Mn5 and Mn particles as inoculants. Under faster cooling weld conditions, the inoculants significantly reduced the length of the columnar dendritic zone, with Ti impacting the most. At the slower cooling rates, the inoculants had little impact on the length of columnar dendritic zone, with all but Al8Mn5 resulting in higher values. The modeling provides additional support the interdependence modeling work applied to Mg alloys [137]. Self-inoculation in (adding solid alloy directly into the melt) 3-7% additions transformed the AZ31 dendritic morphology of the Mg phase into spherical shapes within the slurry [138]. Furthermore, increasing holding time decreased the phase shape factor but coarsened particle size. Phases within resistance welded AZ31were investigated through additions of Al8Mn5 inoculants [139]. Large Al8Mn5 particles of 4 to 10 mu m in length were observed resulting from use of Al8Mn5 as an inoculant, which restricted the growth of columnar grains and promoted equiaxed structures. The addition of 10 um-long Mn particles into the fusion zone during the welding process restrained the growth columnar grains and promoted equiaxed grains. Researchers modified the Gd/Al ratio of AZ61 by introducing Al2Gd as an inoculant [140]. At the ratio of 1, the Al2Gd phase becomes predominant, resulting in intense grain refinement and increasing tensile strength and elongation to failure of Mg-3Gd-3Al-1Zn by similar to 4% and 180% compared with those of AZ61 alloy, respectively. However, at high Gd/Al ratios, the Al2Gd phase was replaced by (Mg, Al)(3)Gd and Mg5Gd phases large grain sizes. This decreased tensile properties and created cleavage facets on fracture surfaces. Like the research involving blown C powders [141], researchers inoculated AZ91, AZ61 and AZ31 magnesium alloys with carbon black powder having an average particle size of 0.042 μm combined with ultrasonic processing [142]. Results indicate ultrasonic treatment helps accelerate the

wetting, de-agglomeration, and dispersion of inoculant particles, resulting in refined microstructures. In AZ91, the yield, UTS, and elongation were increased from 111 MPA, 142 MPA, and 0.07% to 123 MPA, 182 MA, and 0.08, respectively, through inoculation alone. In AZ61, similar increases from 94 MPA, 134 MPA, and 0.06 % to 105 MPA, 174 MPA, and 0.09%. In AZ31 the values increased from 90 MPA, 120 MPA, and 0.09% to 104 MPA, 167 MPA, 0.1%. Du and Wang et al, also studied the impact of carbon inoculation on Mg-3%Al as a function of hold times. They reported holding time had no obvious effect on particle densities, particle size distribution and the mean size of Al-C rich particles in the samples held over 5 min after inoculation. The particles varied in a range of 2-4.5 mu m with a mean size of 2.85 mu m.

A similar alloy (AM30 alloy with 3.4% Al and 0.16% Mn) was inoculated by MgO and MgCO3 [143]. Researchers reported that AM30 alloy could be effectively refined by either MgCO3 or MgO inoculation, with the refining efficiency and fading effect of MgO inoculation were better than those of MgCO3 inoculation. The claim MgAl2O4 should be the potent nuclei of alpha-Mg grain for the AM30 alloy in addition to Al4C3. MgO and MgCO3 did not refine pure Mg. Low levels of Er (60-990 ppm) were also tested in the Mg-6wt% Al casting alloy to understand their modifying effect on Mg17Al12 precipitates [144]. Simulations indicate Al2Er Laves co-precipitates at the same temperature as Mg17Al12, exerting an inoculating effect when Er is at trace levels in the bulk alloy. As Er levels in the alloy increase, Al2Er forms at higher temperatures before Mg17Al12, losing its inoculant potential. It was also seen that Er is soluble in Mg17Al12 causing changes to its lattice parameter and cell volume. At 60 ppm Er, the alloy tensile properties remained similar to the uninoculated control. At 800 ppm, the UTS, yield, and elongation increased slightly from 206 MPA, 74 MPA, and 8% to 211 MPA, 70 MPA, and 10%, respectively. However, the average sizes of Mg17A12 decreased by 56% with 60 ppm Er additions (44% decrease at 800 ppm). The average Mg grain size also decreased by 22% (60ppm) and 18% (800 ppm), with a slight refinement in the dendritic arm spacing. The grain refinement effects of carbon on AZ81 (Mg8%Al) alloys were investigated through the addition of synthetic graphite (21-30um) and activated charcoal (0.04%-0.98wt%) (25-30 um) inoculants [145]. The mean grain size of the alloy was reduced from about 185 to 37 mu m when the C content was increased to 0.98% C. Both tensile strength and ductility increase with increasing carbon content. The yield, UTS, and elongation increased from 79 MPA, 80 MPA, and 2.5% to 97 MPa, 117 MPa, and 2.9 % for the synthetic graphite case, and 193 MPa, 219 MPa, and 6.1% for the 0.98% activated charcoal case. The wear rate also decreased with the increase of C content. Instead of using solid inoculants, researchers studied the effect of C2H2 and CO2 gas inoculation on the grain refinement of AM60B magnesium alloy [146]. Both gases refined the microstructure. C2H2 inoculation decreased the grain size of AM60B alloy from the 412 μm to a minimum 101 μm after holding for 30 min at 760C. Inoculation with CO2 reached the minimum of 92 μm after only 10 min. Holding for longer temperatures increased the grain size. Grain refinement was attributed to the heterogeneous nucleation of Al4C3. Samples treated with CO2 exhibited poorer tensile strength than those treated with C2H2 due to the formation of MgO and MgAl2O4, although both increased the UTS and yield significantly over the unrefined alloy. UTS in C2H2 increased from approximately 140 MPA to 200 MPA, and to 180 MPA in the CO2 case. Elongation increased from approximately 6% to 8% (C2H2) and 7% (CO2). With increasing holding time in melt, the resulting size of Al4C3 particles increased and gradually transformed to the Al-C-Mn phases, resulting in the increased grain size. With the advancement of characterization tools, new insight into nucleation and phase evolution at the atomic scale has become available. This has also led to new models involving inoculation in Mg alloys. For example, the application of advanced focused ion milling and TEM capabilities capture the nucleation crystallography orientation between Mg nuclei

and active Al2Y inoculants in an Mg-10 wt% Y alloy [147]. Results demonstrate Mg can be fully wetted on Al2Y inoculants based on interfacial energy considerations.

In summary, inoculation mainly applied to Mg-9%Al, Mg-6%Al, and Mg-3%Al related alloys, typically involving C, SiC, Mg, and Ti inoculants. The largest tensile strength gains involved C inoculation. Although this also increased elongation properties, these materials have low ductility even with inoculants (<3%).

7. INOCULATIONS IN OTHER ALLOYS

Copper alloys have been important materials for centuries and continue to find use in multiple structural and functional applications. Shape memory alloys are one of the important uses for these materials, and researchers have employed a variety of inoculants to impact properties. For example, an in situ LaB6/Al inoculant was used to significantly refine the grains of a CuAlMn shape memory alloy [148]. Results show the increase in phase interface density improved the damping capacity of the alloy while improving elongation, tensile strength, and yield strength. In similar work, researchers refined the CuAlMn shape memory alloy with CuZr inoculant to investigate the effect of precipitation during aging on microstructure [149]. Other researchers testing CuAlMn report grain refinement through combined use of Cu51Zr14 inoculant and caliber rolling [150]. The improved tensile mechanical properties were ascribed to grain boundary strengthening, decreased mobility of martensite variants, increased difficulty of grain coordination deformation, and the elimination of casting defects. Grains within the SMA Cu-Al-Ni-Mn-Ti were also refined when inoculated with Al-La-B, resulting in the smallest grains with 2.5wt% addition [151]. Damping improvement of was attributed to the increased density of interfaces between martensite lamellae and between twins. In a similar SMA (Cu-Al-Ni), he combined addition of Cu51Zr14 inoculant and Ti decreased the grain size while increasing the damping capacity [152]. However inoculant use in Cu alloys has not been limited to SMAs. For example, inoculants AlZO3 and ZnO added to Cu-Cu2S-X alloys formed dendritic or polyhedral Cu2S by primary crystallization, and rod-like or stringy Cu2S by the eutectic reaction [153]. Without the inoculants, droplets of Cu2S were formed by the monotectic reaction instead of the eutectic reaction. In other research, TiB2 particles were introduced into Cu-Fe melts to produce the TiB2 and Fe2P with nanotwins-reinforced Cu-based immiscible composites by selective laser melting (SLM) [154]. The addition of TiB2 particles refined the size of Fe2P and promoted their homogeneous distribution within the epsilon-Cu matrix. Improvements in hardness and wear resistance were attributed to the combined strengthening mechanisms of twin boundaries (TBs) strengthening, refinement strengthening, dispersion strengthening and precipitation strengthening. The CuNi10Fe1Mn alloy was also refined with SiC nanoparticles coupled with electromagnetic stirring (EMS), modifying grains to a fine equiaxed morphology [155]. The grain size decreased from 2.15mm to 0.52mm, and the impact power is increased about 38.8% compared to that without modified SiC nanoparticles and EMS. X-ray diffraction showed the modified SiC nanoparticles served as heterogeneous nucleation sites directly for CuNi10Fe1Mn alloy.

Inoculants are also being developed and tested for less common applications. For example, Ta particles (size of 5-30 mu m) where used as inoculants to modify the size and distribution of ZrCu-B2 phase in ZrCuAlCo-based bulk metallic glass composites (BMGC) [156]. The resulting microstructure provided significantly improved mechanical properties (1890 MPa fracture stress and 14% plastic strain) in comparison with the base BMGC (1560 MPa fracture strength and 7.5% plastic strain) through manipulation of the TRIP-effect enabled through ZrCu-B2 distribution. Researchers have also used

inoculants to create Si3N4 precipitates in solar sell Si materials [157], and nanosize Y2O3 powder additions in HEAs to form core-shell structures [158]. Even Sn solders have been inoculated to promote beta-Sn nucleation in near eutectic Sn-Ag-Cu solders as a strategy for avoiding development of unwanted microconstituents [159]. Inoculation in Pb-Sn test castings served as heterogeneous nucleation sites for equiaxed crystals that were transported through the vertically solidifying melt [160].

8. SUMMARY

In each of the material systems (Steel and Cast Iron, Al, Ti, Ni, Mg and Cu), the addition of inoculants significantly improved mechanical properties and refined/modified microstructures and or phases. This is expected in casting alloys given the continued advancement of alloy melts and improvements in mechanical and ultrasonic mixing technologies. However, advancements in additive manufacturing and laser processing have generated additional interest in controlling chemical homogeneity and grain/phase morphologies under rapid cooling conditions. Inoculants address these issues by modifying solidification conditions and localized chemistries, as demonstrated in steel and Ti alloys where additions helped transition from columnar to equiaxed grains in direct energy deposition systems. Improvements in corrosion, wear resistance, hardness, grain size, defect reduction, and phase morphology have been realized. New feedstock materials are possible, including many materials such as high entropy alloys and complex oxide particles that are being used as novel inoculants. The use of these materials remains to be optimized to determine overall effectiveness. With the potential to increase strength and corrosion properties at higher temperatures and loads, the use of inoculants should be monitored with regard to potential missile applications. The ability to employ inoculants in high strength materials under near net shape casting approaches may provide an inexpensive alternative to high cost maraging steels that require machining of wrought materials. Improved castability of these high strength alloys may address current MCTR limitations concerning alloy product forms.

9. REFERENCES

1. Fleeman, EL; Missile Design Guide, AIAA Education Series, 2022
2. Miracle, DB; Nature Communications, 10, 1805, 2019
3. Miracle, DB; O.N. Senkov, Refractory Complex Concentrated Alloys, ARPA-E Workshop, 2019
4. Missile Technology Control Regime TEM Annex, 2021
5. Sha, W.; Steels, Springer, London, 2013
6. Martin, J; Yahata, B; Hundley, J; Mayer, J; Schaedler, T; Pollock, T; Nature, v 549, 2017
7. Callister W, Materials Science and Engineering an Introduction, John Wiley & Sons, 2007
8. Askeland D, et al., The Science and Engineering of Materials, Sixth Edition, Cengage Learning, 2011
9. Campbell. J; Complete Casting Handbook, 2nd Edition, Elsevier, 2015
10. Jung, JG; Ahn, TY; Cho, YH; Kim, SH; Lee, JM, Acta Mat., v 144, 2018
11. Quested, TE, Acta Mat., 2004
12. Murty, Bs, Kori, SA, and Chakraborty, M, Int. Mat. Reviews, 2013
13. Quested, TE; Greer, AL, Acta Mat., v 52, iss 13, 2004
14. Quested, TE; Greer, AL, Acta Mat., v 53, iss 17, 2005
15. Qi, XB; Chen, Y; Kang, XH; Li, DZ; Du, Q, Acta Mat., v 99, 2015
16. StJohn, DH; Qian, M; Easton, MA; Cao, P, Acta Mat., v 59, iss 12, 2011
17. Wang, F; Liu, ZL; Qiu, D; Taylor, JA; Easton, MA; Zhang, MX, Met. Mat. Trans A, v 46A, iss 1, 2015
18. Wearing, D; Horsfield, AP; Xu, WW; Lee, PD, J. of Alloys and Compounds, v 664, 2016
19. Colombo, M; Gariboldi, E; Morri, A, Structural Mat. Prop., v 713, 2018
20. Liu, SQ; Wang, X; Cui, CX; Zhao, LC; Liu, SJ; Chen, C, Mat. & Design, v 65, 2015
21. Liu, SQ; Cui, CX; Wang, X; Li, N; Shi, JJ; Cui, S; Chen, P, Metals, v 7, iss 6, 2017
22. Birol, Y, J. of Alloys and Compounds, V 430, iss 1-2, 2007
23. Vandyoussefi, M; Worth, J; Greer, AL, Mat. Sci, and Tech., v 16, iss 10, 2000
24. Wang, K; Cui, CX; Wang, Q; Qi, YM; Wang, C, J. of Alloys and Compounds, v 547, 2013
25. Wang, Q; Wang, X; Cui, CX; Zhao, LC; Liu, SJ, Adv. Eng. Mat., v 19, iss 1, 2017
26. Jung, JG; Cho, YH; Kim, SD; Kim, SB; Lee, SH; Song, K; Euh, K; Lee, JMt, Acta Mat.,v 199, 2020
27. Okle, P; Lin, JD; Zhu, TY; Dunand, DC; Seidman, DN, Mat. Sci. and Eng. A, v 739, 2019
28. Ding, JH; Cui, CX; Sun, YJ; Shi, JJ; Cui, S; Ma, Q, Mat. Sci and Eng. A, v 738, 2018
29. Gao, T; Zhu, XZ; Qiao, H; Liu, XF., J. of Alloys and Compound, v 607, 2014
30. Zhang, L; Eskin, DG; Katgerman, L, J. of Mat Sci., v 46, iss 15, 2011
31. Xu, YJ; Casari, D; Du, Q; Mathiesen, RH; Arnberg, L; Li, YJ, Acta Mat., v 140, 2017
32. Geng, HT; Cui, CX; Liu, L; Liang, YG, J. of Alloys and Compounds, v 903, 2022
33. Ram, GDJ; Mitra, TK; Raju, MK; Sundaresan, S, Mat. Sci. and Eng. A, v 256, iss 1-2, 2000
34. Tan, QY; Zhang, JQ; Sun, Q; Fan, ZQ; Li, G; Yin, Y; Liu, YG; Zhang, MX, Acta Mat., v 196, 2020
35. Colombo, M; Gariboldi, E; Morri, A, Structural Mat. Prop., v 713, 2018
36. Fan, ZH; Yan, XC; Fu, ZY; Niu, B; Chen, JF; Hu, YJ; Chang, C; Yi, JL, Vacuum, v 188, 2021

37. Tan, QY; Yin, Y; Fan, ZQ; Zhang, JQ; Liu, YG; Zhang, MX, Mat. Sci. and Eng. A, v 800, 2021
38. Gao, T; Zhang, SY; Liu, GL; Sun, QQ; Liu, JW; Sun, QD; Sun, J; Wang, ZC; Liu, XF; Wang, XB, Materialia, v 16, 2021
39. Xu, J; Li, RX; Li, Q, Met. Mat. Trans A, v 52, iss 3, 2021
40. Kyffin, WJ; Rainforth, WM; Jones, H, Mat. Sci. and Tech, v 17, iss 8, 2001
41. Sreekumar, VM; Babu, NH; Eskin, DG, J. of Mat. Eng. And Performance, v 26, iss 9, 2017
42. Pineda, DA; Martorano, MA, Acta Mat., v 61, iss 5, 2013
43. Hu, BH; Li, H, J. Mat. Proc. Tech., v 74, iss 1-3, 1998
44. Rao, AKP; Das, K; Murty, BS; Chakraborty, M, J. of Alloys and Compounds, v 480, iss 2, 2009
45. Li, QL; Zhao, S; Bao, XP; Zhang, YS; Zhu, YQ; Wang, CZ; Lan, YF; Zhang, YX; Xia, TD, J. of Mat. Sci. and Tech, v 52, 2020
46. Li, QL; Zhao, S; Li, BQ; Zhu, YQ; Wang, CZ; Lan, YF; Xia, TD, Mat. Letters, v 251, 2019
47. Li, Y; Hu, B; Gu, QF; Liu, B; Li, Q, Scripta Mat., v 160, 2019
48. Nowak, M; Bolzoni, L; Babu, NH, J. of Alloys and Compounds, v 641, 2015
49. Liu, SQ; Wang, X; Tao, YR; Han, X; Cui, CX, Applied Surface Sci, v 484, 2019
50. Nagaraja, S; Nagegowda, KU; Kumar, VA; Alamri, S; Afzal, A; Thakur, D; Kaladgi, AR; Panchal, S; Saleel, CA, Materials, v 14 iss 9, 2021
51. Schempp, P; Schwenk, C; Rethmeier, M; Cross, CE, Mat. Testing, v 53, iss 10, 2011
52. Zakharov, VV, Metal Sci and Heat Treatment, v 45, iss 7-8, 2003
53. Schempp, P; Cross, CE; Pittner, A; Oder, G; Neumann, RS; Rooch, H; Dörfel, I; Österle, W; Rethmeier, M, Welding Journal, v 93, iss 2, 2014
54. Schempp, R; Cross, CE; Schwenk, C; Rethmeier, M, Welding in the World, v 56, iss 9-10, 2012
55. Fayomi, OSI; Gbenebor, OP; Abdulwahab, M; Bolu, CA; Popoola, API, J. of New Mat. For Electrochemical Sys., v 16, iss 1, 2013
56. De Cicco, MP; Turng, LS; Li, XC; Perepezko, JH, Met. Mat Trans A, v 42A, iss 8, 2011
57. Nafisi, S; Ghomashchi, R, Mat. Sci. and Eng. A, v 452, 2007
58. Rao, AKP; Das, K; Murty, BS; Chakraborty, M, Mat. Letters, v 62, iss 2, 2008
59. Li, N; Liu, XJ; Wang, QZ; Cui, CX; Yin, FX; Ji, XW; Jiao, ZX, Mat. & Design, v 127, 2017
60. Wang, ZC; Wang, XT; Chen, X; Qiu, CL, Additive Manufacturing, v 51, 2022
61. Xiao, F; Wang, SB; Wang, YX; Shu, D; Zhu, GL; Sun, BD; StJohn, D, J. of Alloys and Compounds, v 900, 2022
62. Zhu, ZG; Ng, FL; Seet, HLH; Lu, WJ; Liebscher, C; Rao, ZY; Raabe, D; Nai, SML, Materials Today, v 52, 2022
63. Sun, Q; Jiang, HX; Zhao, JZ; He, J, Acta Mat., v 129, 2017
64. Sun, Q; Jiang, HX; Zhao, JZ; He, J, Mat. & Design, v 91, 2016
65. Kaban, I; Köhler, M; Ratke, L; Hoyer, W; Mattern, N; Eckert, J; Greer, AL, Acta Mat., v 59, iss18, 2011
66. Byun, JS; Shim, JH; Cho, YW, Scripta Mat., v 48, iss 4, 2003
67. Durga, A, Pettersson, NH, et al., Scripta Mat., v 194, 2021
68. Poole, WJ; Mitchell, A; Weinberg, F, High Temp. Mat. And Properties, v 16, iss 3, 1997
69. Park, JH, CALPHAD-Computer Coupling of Phase Diagrams and Thermochemistry,

2011, v 35, iss 4
70. Villaret, V; Deschaux-Beaume, F; Bordreuil, C, J. of Mat. Proc. Tech, v 233, 2016
71. Chaus, AS, Mat. Sci and Tech, v 30, iss 9, 2014
72. Chaus, AS, ISIJ Int., v 45, iss 9, 2005
73. Li, N; Cui, CX; Zhao, YQ; Zhang, QX; Bai, LN, MSE-A, v 738, 2018
74. Riposan, I; Chisamera, M; Stan, S, China Foundry, v 11, iss 4 , 2014
75. Chisamera, M; Riposan, I; Stan, S; Militaru, C; Anton, I; Barstow, M, J. of Mat Eng and Performance, v 21 iss 3, 2012
76. Kim, EH; Cho, GH; Lee, JH; Jung, YG; Yoo, Y; Seo, S, Ceramics Int., v 39, iss 6, 2013
77. Chisamera, M; Riposan, I; Stan, S; Toboc, P; Skaland, T; White, D, J. of Cast Metals Research, v 24, iss 1, 2011
78. Muhmond, HM; Fredriksson, H, Met. Mat. Trans B, v 44, iss 2, 2013
79. Sommerfeld, A; Tonn, B, Int. J. of Cast Metals Research, v 21, iss 1-4, 2008
80. Alonso, G; Larrañaga, P; la Fuente, E; Stefanescu, DM; Natxiondo, A; Suarez, R, Int J. of Metalcasting, v 11, iss 1, 2017
81. Svensson, IL; Millberg, A; Dioszegi, A, Int. J. of Cast Metals Research, v 16, iss 1-3, 2003
82. Wang, GQ; Chen, X; Li, YX; Liu, ZL, Materials, v 11, iss 10, 2018
83. Xue, WD; Li, Y, J. of Alloys and Compounds, v 689, 2016
84. Foglio, E; Lusuardi, D; Pola, A; La Vecchia, GM; Gelfi, M, Materials and Design, v 111, 2016
85. Borsato, T; Ferro, P; Berto, F, Fatigue and Fracture of Eng. Mat., v 41, iss 8, 2018
86. Ferro, P; Fabrizi, A; Cervo, R; Carollo, C, J. of Mat. Proc. Tech., v 213, iss 9, 2013
87. Regordosa, A; de la Torre, U; Loizaga, A; Sertucha, J; Lacaze, J, China Foundry, v 7, iss 2, 2010
88. Riposan, I; Chlsamera, M; Stan, S, China Foundry, v 4, iss 4, 2007
89. Riposan, I; Chisamera, M; Stan, S, China Foundry, v 7, iss 2, 2010
90. Heidari, E; Boutorabi, SMA; Honaramooz, MT; Campbell, J, Int. J of Metalcasting, v 16, iss 1, 2022
91. Stan, S; Riposan, I; Chisamera, M; Stan, I, J. of Mat. Eng. and Performance, v 28, iss 1, 2019
92. Chisamera, M; Riposan, I; Stan, S; Toboc, P; Skaland, T; White, D, J. of Cast Metals Research, v 24, iss 1, 2011
93. Alonso, G; Larrañaga, P; la Fuente, E; Stefanescu, DM; Natxiondo, A; Suarez, R, Int J. of Metalcasting, v 11, iss 1, 2017
94. Asensio-Lozano, J; Alvarez-Antolín, JF; Voort, GFV, J. of Mat Proc Tech, v 206, iss 1-3 , 2008
95. Yilmaz, SO; Teker, T, J. of Alloys and Compounds, v 672, 2016
96. Bartlett, LN; Avila, BR, Int. J. of Metalcasting, v 10, iss 4, 2016
97. Park, JS; Lee, C; Park, JH, Met Mat Trans B, v 43, iss 6 (2012)
98. Dojka, M; Dojka, R; Stawarz, M; Studnicki, A, J. of Mat. Eng. Performance, v 28, iss 7 , 2019
99. Chung, RJ; Tang, X; Li, DY; Hinckley, B; Dolman, K, Wear, v 267, iss 1-4, 2009
100. Nishizawa, T, ISIJ International, v 40, iss 12, 2000
101. Dou, K; Meng, LT; Liu, Q; Liu, B; Huang, YH, Metals & Materials Int., v 22, iss 3, 2016
102. Ma, FJ; Wen, GH; Wang, WL, Steel Research Int., v 84, iss 4, 2013
103. Chisamera, M; Riposan, I; Stan, S; Militaru, C; Anton, I; Barstow, M, J. of Mat Eng and Performance, v 21 iss 3, 2012

104. Fras, E; López, HF; Podrzucki, C, Int. J. of Cast Metals Research, v 13, iss 2, 2000
105. Rodrigues, TA; Duarte, VR; Tomás, D; Avila, JA; Escobar, JD; Rossinyol, E; Schell, N; Santos, TG; Oliveira, JP, Additive Manufacturing, v 34, 2020
106. Sommerfeld, A; Tonn, B, Int. J. of Metalcasting, v 3, iss 4, 2009
107. Vicente, AD; Moreno, JRS; Santos, TFD; Espinosa, DCR; Tenório, JAS, J. of Alloys and Compounds, v 775, 2019
108. Wakoh, M; Sawai, T; Mizoguchi, S, ISIJ International, v 36, iss 8, 1996
109. Wakoh, M; Sawai, T; Mizoguchi, S, J. of Iron and Steel Institute of Japan, v 78, iss 11, 1992
110. Ma, FJ; Wen, GH; Wang, WL, Steel Research Int., v 84, iss 4, 2013
111. Chisamera, M; Riposan, I; Stan, S; Militaru, C; Anton, I; Barstow, M, J. of Mat Eng and Performance, v 21 iss 3, 2012
112. Fras, E; López, HF; Podrzucki, C, Int. J. of Cast Metals Research, v 13, iss 2, 2000
113. Alonso, G; Larrañaga, P; Stefanescu, DM; Suarez, R, Int J of Metalcasting, v 14, iss 4, 2020
114. Sommerfeld, A; Böttger, B; Tonn, B, J. of Mat. Sci and Tech., v 24, iss 3, 2008
115. Ho, IT; Chen, YT; Yeh, AC; Chen, CP; Jen, KK, Additive Manufacturing, v 21, 2018
116. Ho, IT; Hsu, TH; Chang, YJ; Li, CW; Chang, KC; Tin, S; Kakehi, K; Yeh, AC, Additive Manufacturing, v 35, 2020
117. Xiong, YH; Du, J; Wei, XY; Yang, AM; Liu, L; Zeng, DB, Met. And Mat. Trans A, v 35A, iss 7, 2004
118. Jin, WZ; Bai, FD; Li, TJ; Yin, GM, Materials Letters, v 62, iss 10-11, 2008
119. Matysiak, H; Zagorska, M; Balkowiec, A; Adamczyk-Cieslak, B; Dobkowski, K; Koralnik, M; Cygan, R; Nawrocki, J; Cwajna, J; Kurzydlowski, K; JOM, v 68, 00 185-197, 2016
120. Rakoczy, L; Grudzien, M; Cygan, R, J. of Mat. Eng. And Perf., v 35A, iss 7, 2019
121. Zhen, BL; Liu, L; Zhong, ZY; BanerjiI, A; Reif, W, Metall, v 48, iss 2, 1994
122. Pinomaa, T; Yashchuk, I; Lindroos, M; Andersson, T; Provatas, N; Laukkanen, A, Metals, v 9, iss 11, 2019
123. Kennedy, JR; Davis, AE; Caballero, AE; Williams, S; Pickering, EJ; Prangnell, PB, Additive Manufacturing, v 40, 2021
124. Li, N; Cui, CX; Liu, SJ; Liu, SQ; Cui, S; Wang, Q, Metal, v 7, iss 7, 2017
125. Kennedy, JR; Daloz, D; Rouat, B; Bouzy, E; Zollinger, J, Intermetallics, v 95, 2018
126. Huang, DN; Tan, QY; Zhou, YH; Yin, Y; Wang, F; Wu, T; Yang, XL; Fan, ZQ; Liu, YG; Zhang, JQ; Huang, H; Yan, M; Zhang, MX, Additive Manufacturing, v 46, 2021
127. Cui, S; Cui, CX; Yang, SC; Liu, SJ, Met. Sci. & Eng. A, v 829, 2022
128. Kartavykh, AV; Gorshenkov, MV; Podgorny, DA, Materials Letters, V 142, 2015
129. Lu, JW; Zhao, YQ; Du, Y; Zhang, W; Zhang, YS, J. of Alloys and Compounds, v 778, 2019
130. Chen, SN; Yang, W; Yu, H; Zhang, YL, J. of Alloys and Compounds, v 611, 2014
131. Motegi, T; Yano, E; Tamura, Y; Sato, E, Magnesium Alloys 2000, v 350-3, 2000
132. Emadi, P; Andilab, B; Ravindran, C, Mat. Sci. & Eng. A, v 819, 2021
133. Xiao, L; Liu, L; Esmaeili, S; Zhou, Y, Met. And Mat. Trans A, v 43A, iss 2, 2012
134. Jiang, B; Liu, WJ; Qiu, D; Zhang, MX; Pan, FS, Mat. Chem. & Physics, v 133, iss 2-3, 2012 Prabhu, TR, J. of Mat. Research and Tech., v 5, iss 3, 2016
135. Günther, R; Hartig, C; Bormann, R, Acta Mat., v 54, iss 20, 2006
136. Montiel, D; Liu, L; Xiao, L; Zhou, Y; Provatas, N, Acta Mat.,v 60, iss 16, 2012
137. StJohn, DH; Qian, M; Easton, MA; Cao, P, Acta Mat., v 59, iss 12, 2011
138. Xing, B; Hao, Y; Li, YD; Ma, Y; Chen, TJ, Trans of Nonferrous Metals Society of

China, v 23, iss 3, 2013
139. Xiao, L; Liu, L; Zhou, Y; Esmaeili, S, Met. And Mat. Trans A, v 41A iss 6, 2010
140. Pourbahari, B; Emamy, M; Mirzadeh, H, Prog. In Nat. Sci-Mat. Int., v 27, iss 2, 2017
141. Motegi, T; Yano, E; Tamura, Y; Sato, E, Magnesium Alloys 2000, v 350-3, 2000
142. Bhingole, PP; Chaudhari, GP, Mat. Sci & Eng. A, v 556, 2012
143. Du, J; Yao, ZJ; Han, S; Li, WF, J. od Magnesium and Alloys, V 5, iss 2, 2017
144. Korgiopoulos, K; Langelier, B; Pekguleryuz, M, Mat. Sci. & Eng. A, v 812, 2021
145. Prabhu, TR, J. of Mat. Research and Tech., v 5, iss 3, 2016
146. Tong, X; You, GQ; Liu, Y; Long, SY; Liu, Q, J. of Mat. Proc. Techn., v 271, 2019
147. Qiu, D; Zhang, MX., J. of Alloys and Compounds, v 586, 2014
148. Liu, XJ; Wang, QZ; Kondrat'ev, SY; Ji, PG; Yin, FX; Cui, CX; Hao, GL, Met. And Mat. Trans A, v 50A, iss 5, 2019
149. Jiao, ZX; Wang, QZ; Yin, FX; Cui, CX, Mat. Sci. and Eng. A, v 737, 2018
150. Jiao, ZX; Wang, QZ; Yin, FX; Cui, CX; Zhang, JJ; Yao, C, Mat. Sci., and Eng. A, v 772, 2020
151. Yao, C; Yin, FX; Ji, PG; Hao, GL; Jiao, ZX; Liu, L; Zhang, JJ; Cui, CX; Wang, QZ, Intermetallics, v 138, 2021
152. Ding, YJ; Wang, QZ; Yin, FX; Cui, CX; Hao, GL, Mat. Sci. and Eng. A, v 743, 2019
153. Oikawa, K; Kawashita, Y; Ohtani, H; Ishida, K; Nishizawa, T, J. of Japan Inst. of Metals, v 59, v 12, 1995
154. Xie, M; Wu, CY; Zhou, SF; Jin, JB; Zhao, SZ; Chen, DC, J. of Alloys and Compounds, v 864, 2021
155. Yan, ZM; Chen, ML; Yang, J; Yang, L; Gao, H, Mat. And Man. Processes, v 28, iss 8, 2013
156. Liao, YC; Song, SM; Li, TH; Chiang, YL; Tsai, PH; Nguyen, VT; Li, SY; Jang, JSC; Huang, JC, J. of Alloys and Compounds, v 774, 2019
157. Brynjulfsen, I; Arnberg, L; Autruffe, A, J. of Crystal Growth, v 361, 2012
158. Zhang, H; Wu, WF; He, YZ; Li, MX; Guo, S, Applied Surf. Sci., v 363, 2016
159. Zhang H; Wu, WF; Macromolecular Rapid Comm., v 26 (16) pp 1341-1345, 2005
160. Zheng, Y; Wu, M; Kharicha, A; Ludwig, A, Computational Mat. Sci., v 124, 2016